

A UNIFORM ANALYSIS OF THE LY- α FOREST AT Z=0 - 5:
I. THE SAMPLE AND DISTRIBUTION OF CLOUDS AT Z > 1.7

JENNIFER SCOTT¹, JILL BECHTOLD¹, & ADAM DOBRZYCKI²

To appear in the September 2000 Astrophysical Journal Supplement Series

ABSTRACT

We present moderate resolution data for 39 quasi-stellar objects (QSOs) at $z \approx 2$ obtained at the Multiple Mirror Telescope. These data are combined with spectra of comparable resolution of 60 QSOs with redshifts greater than 1.7 found in the literature to investigate the distribution of Ly α forest lines in redshift and equivalent width. We find a value for γ , the parameter describing the number distribution of Ly α forest lines in redshift, of 1.88 ± 0.22 for lines stronger than a rest equivalent width of 0.32 \AA , in good agreement with some previous studies. The Kolmogorov-Smirnov test was applied to the data and it is found that this single power law is a good fit over the relevant redshift ranges. Simulations of the Lyman α forest were performed to determine the completeness of the line lists and to test how well the analysis recovers the underlying line statistics, given this level of completeness.

Subject headings: quasars: absorption lines

1. INTRODUCTION

The spectra of quasi-stellar objects (QSOs) blueward of Ly α emission show a large number of absorption lines primarily due to Ly α absorption by intervening neutral hydrogen along the line of sight to the QSO (Lynds, 1971; Sargent et al. 1980; Weymann, Carswell, & Smith, 1981). The evolution of the number density of these lines can be described by a power law in $1+z$ with index γ . It has been debated whether the number densities of absorbers of different column densities, Lyman α forest, Lyman limit systems, and damped Lyman α systems, evolve differently with redshift which would indicate that these absorbing structures represent different populations of objects (Lanzetta 1991, Storrie-Lombardi 1994,1995, Giallongo et al. 1996).

Several authors have carried out the analysis of the statistics of the Lyman α forest on other data sets (Lu et al. 1991, hereafter LWT; Bechtold 1994, hereafter B94; Williger et al. 1994; Cristiani et al. 1995; Giallongo et al. 1996; Kim et al. 1997; Weymann et al. 1998.) At high redshift, LWT find $\gamma = 2.75 \pm 0.29$; and B94, whose resolution class M sample is a subsample of our total sample, finds $\gamma = 1.85 \pm 0.27$. These results were obtained using a fixed equivalent width threshold of 0.36 \AA and using only Ly α lines outside the immediate vicinity of the QSO. Work with high resolution spectra has yielded results similar to those of both LWT and B94. Cristiani et al. (1995) find $\gamma = 1.86 \pm 0.21$ for Lyman α forest lines with $\log(N_{HI}) \geq 13.8$ from $R \sim 22,000$ spectra of 3 QSOs; and Giallongo et al. (1996) find $\gamma = 2.7$ for lines with $\log(N_{HI}) \geq 14$ from $R \sim 25,000$ spectra of 10 QSOs. Similarly, Kim et al. (1997) report $\gamma = 2.78$ from a sample of $R \sim 36,000$ spectra of 5 QSOs taken using the HIRES Spectrograph on the Keck Telescope.

The evolution is significantly flatter at redshifts less than 1.7. The first Hubble Space Telescope Quasar Absorption

Line Key Project paper (Bahcall et al. 1993) reported $\gamma = 0.50 \pm 0.77$ for lines from 13 objects with $W > 0.32 \text{ \AA}$. The addition of four more quasars at $z < 1.3$ yielded $\gamma = 0.58 \pm 0.50$ for lines with $W > 0.24 \text{ \AA}$ (Bahcall et al. 1996). Weymann et al. (1998) have analyzed the complete HST Key Project Ly α -absorption line sample presented by Jannuzi et al. (1998). They find $\gamma = 0.15 \pm 0.23$ for a fixed equivalent width threshold of 0.24 \AA . From a large sample of archival HST/Faint Object Spectrograph (FOS) spectra which includes the public data from the Key Project, Dobrzycki & Bechtold (1997) find $\gamma = 0.87 \pm 0.27$ for lines with $W > 0.36 \text{ \AA}$ at $z < 1.7$, and notes that this value flattens to $\gamma = 0.14 \pm 0.45$ for Ly α lines with equivalent widths between 0.24 and 0.36 \AA . This is supported by Weymann et al. (1998) who also find a trend of increasing γ with increasing line strength.

In this paper, a homogeneous sample of moderate resolution QSO spectra is used to investigate the number density evolution of Ly α systems and how this changes with redshift and with varying equivalent width thresholds. Specifically, the Ly α forest in the redshift range between 1.6 and 2.0 was targeted because few lines of sight in the literature cover this range, as it extends down to wavelengths of $\sim 3200 \text{ \AA}$. Improvements in CCD technology allowed us to obtain data in this spectral region. We present new data for 39 objects and supplement this sample with 60 objects from the literature. Metal line systems in these spectra have been identified and removed from the final analysis of the Ly α forest (Murdoch et al. 1986, hereafter MHPB). The resulting Ly α absorption line sample is comprised of 2079 lines in the range $1.6 < z < 4.1$ when a variable equivalent width threshold is used, or 1131 lines using a fixed rest equivalent width threshold of 0.32 \AA . Future papers will extend this work to the local universe using a sample of low-redshift spectra from the HST/Faint Object Spectrograph (FOS) archives.

¹Steward Observatory, University of Arizona, Tucson, AZ 85721, USA
e-mail: [jscott,jbechtold]@as.arizona.edu

²Harvard-Smithsonian Center for Astrophysics, 60 Garden Street, Cambridge, MA 02138, USA
e-mail: adobrzycki@cfa.harvard.edu

Much recent work has promoted treating the Ly α forest as density fluctuations in the continuous field of the intergalactic medium (Bi 1993; Reisenegger & Miralda-Escudé 1995; Hernquist et al. 1996; Miralda-Escudé et al. 1996; Bi & Davidsen 1997; Croft et al. 1998,1999; Weinberg et al. 1999). However, in this paper, we will continue to interpret the Ly α forest as a series of discrete lines for comparison to previous work. The spectra presented in this data set will be of particular use to those interested in using the Ly α forest to recover the power spectrum of mass fluctuations in the universe (Croft et al. 1998,1999) and are available on the web. For the spectra used in this paper, see the authors' homepages, which are accessible from either <http://www.as.arizona.edu> or <http://cfa-www.harvard.edu>.

In Section 2, the details of the observations are outlined and the absorption line sample is presented. Notes on individual sample QSOs and their corresponding absorption line systems are given in Section 3. In Section 4 the statistics of the Ly α forest are derived and discussed. Lyman α forest simulations based on our sample of QSOs were performed to test the ability of our analysis to recover the underlying line statistics in our moderate resolution data. These are also presented and discussed in Section 4. In a subsequent paper, Paper II in this series (Scott, Bechtold, Dobrzycki, & Kulkarni 2000), we will investigate the measurement of the mean intensity of the ionizing background radiation using this Ly α forest sample.

2. DATA

2.1. Observations and Data Reduction

A sample of 39 QSOs was observed using the Multiple Mirror Telescope and Blue Channel Spectrograph. The observations are summarized in Table 1. Each object's redshift is given in column (3) and the reference for that redshift is given in column (4).

The three instrumental setups used are as follows: (1) the "Big Blue" image tube and photon counting Reticon detector, a 832 l mm⁻¹ grating blazed at 3900 Å in the second order with a CuSO₄ red blocking filter, and a 1" × 3" slit; (2) the 3K × 1K CCD, the 832 l mm⁻¹ grating blazed at 3900 Å in the second order with a CuSO₄ order blocking filter, and a 1" × 180" slit; and (3) the 3K × 1K CCD, 800 l mm⁻¹ grating blazed at 4050 Å in the first order, and a 1" × 180" slit. All these spectra have a spectral resolution of ~1 Å with the exception of the spectra of 1207+399 and 1408+009 taken with the 800 l mm⁻¹ grating, which have a resolution of ~2.5 Å. Thinning and backside illumination of a Loral CCD along with the use of antireflection coatings and backside surface charging (Lesser 1994) improved the quantum efficiency of the 3K × 1K CCD used to over 80% at 3200 Å. The exposures from the first runs using the improved CCD at the MMT suffer from a variable focus across the chip due to problems with the original field flatteners used. Figure 1 shows the FWHM of the comparison lamp lines as a function of wavelength. The July 1993 data was taken on the first run with this CCD detector; and a number of problems were encountered, including poor charge transfer efficiency and a jump in the bias level of ~8 ADU in the center of the chip. On this run, the FWHM rises to ~2.5 Å at the red end of the spectrum (short-dashed line

in Figure 1).

Wavelength calibration was performed using He-Ne-Ar-Hg-Cd lamp exposures; and domeflats or quartz exposures were used to correct for pixel-to-pixel variations. When available, a few half-hour exposures of each object are combined; and the total integration time is listed in Table 1. The QSO spectra are available in HTML and Postscript format at <http://qso.as.arizona.edu/~jscott/Spectra/index.html>.

Cosmic rays were removed from the data during the reduction process. Bad columns on the CCD were left in the spectrum in order to keep track of their positions. The flux in these regions was set to a value of -1000.; and they were excluded from the analysis. In some spectra, some clearly non-Gaussian features are present at the red end, mainly redward of Lyman α emission. Because these features occur at the same pixel in each of the spectra in which they are visible, they are identified as traps in the CCD. They are discussed individually in Section 3 below.

2.2. Line Identification Process

The continuum was fit iteratively to each spectrum and significant (3σ or greater) absorption lines were found by measuring the equivalent width in bins of size equal to 2.46 times the FWHM of the comparison lines in pixels, the point at which a Gaussian is 1.5% of its peak value (B94, Young et al. 1979). Lines of 3σ significance and above were used to help identify metal line systems, but only lines of greater than 5σ significance were used in the analysis of the Lyman α forest statistics.

Using the technique described in Dobrzycki and Bechtold (1996), we produced a set of 30 simulated $z=2.48$ pure Ly α forest spectra in order to determine how reliably our program for finding significant lines, FINDSL, recovers those generated by the simulations. We use values of 1.82 and 1.46 for Ly α forest statistics γ and β , but the results of this analysis should not be sensitive to the value of γ as the redshift path covered in each spectrum is small. The lower and upper column density limits chosen were 1×10^{12} and 7×10^{14} cm⁻² respectively; and the mean Doppler parameter and width of the Doppler parameter distribution used were 28 km s⁻¹ and 10 km s⁻¹. The column density limits were chosen to give the same total absorption in the simulated spectra as is seen in the spectrum of 0955+472, the object spectrum which served as the template for this series of simulations.

We determine matches between the simulation line list output and the FINDSL line lists on the basis of the best wavelength match between simulated and recovered lines. At 5σ significance, the line lists are 55% complete. When blending is accounted for by matching all simulated lines within 2.46 resolution elements of each recovered line to that recovered line, 99% of the lines in the simulation are recovered. These completeness values for 3σ lines are 49% and 98% respectively. Obviously, FINDSL can do nothing to help us overcome the finite resolution of the data, but when this is taken into consideration, this test indicates that it does a good job of recovering the lines it is capable of recovering.

Our simulations also revealed another interesting point. Of the 3σ lines "recovered" by FINDSL, a small percentage, ~0.25%, were not generated by the simulation program. In other words, FINDSL found some lines in the

noise. This was not true of the 5σ lines, however, so we expect no spurious lines to be present in the line lists used for the analysis of Lyman α forest statistics. We do use lines with significance levels between 3σ and 5σ for metal line identification purposes; but expect that any low occurrence of spurious lines would have no effect on those identifications due to the all the constraints that were placed upon metal line matches to qualify as true metal line systems, which are discussed in more detail below.

The July 1993 CCD data suffers from a gradient in the FWHM across the spectrum as discussed in Section 2, rising from $\sim 1.1 \text{ \AA}$ in the blue end to $\sim 2.5 \text{ \AA}$ in the red (Figure 1). This variation has some impact on how FINDSL identifies significant lines. Using a FWHM of 2.5 \AA for $\lambda > 3700 \text{ \AA}$, results in fewer significant lines identified relative to the case where a FWHM of 1.1 \AA is used over the full spectrum. Inspection of the fits for these two cases for several objects in our sample leads us to conclude that the two cases give consistent total equivalent widths for absorption features, but that using a search window based on a FWHM of 1.1 \AA , even at the red ends of these spectra, gives the most reasonable line identifications, as the larger window tended to blend distinct features together. Table 2 gives a list of the vacuum, heliocentric wavelengths of all lines identified along with the equivalent width of each line as determined by a Gaussian fit to the line.

We generated additional synthetic Ly α forest spectra with no metal lines in order to determine the maximum number of metal line identifications that our software will identify spuriously in the Ly α forest, or equivalently, the minimum number of metal line identifications needed to qualify as a metal line system, cf. Dobrzycki and Bechtold (1996). The simulation parameters used in this case were $\gamma=1.5$, $\beta=1.46$, $N_{lower}=2 \times 10^{12} \text{ cm}^{-2}$, $N_{upper}=10^{16} \text{ cm}^{-2}$, $\langle b \rangle = 28 \text{ km s}^{-1}$, and $\sigma_b = 10 \text{ km s}^{-1}$. We find that our program will find metal line systems in the Lyman α forest that may appear to be reasonable based on the species present and doublet ratios, if the number of required matches between the data and a table of possible metal lines is set to a number less than four if there are less than ~ 100 lines in the spectrum, and less than five if there are more than ~ 100 identified lines in the spectrum. If a system shows lines redward of Ly α emission, this requirement is relaxed since this spectral region is free of Ly α forest absorption lines.

The search list of metal lines, their wavelengths, and their f values was taken from Table 4 of Morton et al. (1988) supplemented with Fe II $\lambda 1143$ and $\lambda 1145$ and N I $\lambda 1135$ from their Table 3. Redshift systems were identified by first running our metal line searching program to find systems with our prescribed number of matches. Metal line matches within 3σ of an observed significant line are counted. The output of this program was analyzed for consistency with required doublet ratios and f values. Lines found by this program were rejected if a) the weaker line of a doublet is detected while the stronger is not or b) a weak line of a species is detected while a stronger line of the same species and ionization state is not (eg. Si II $\lambda 1304$ is detected but Si II $\lambda 1260$ is not). Next, lines with rest equivalent width greater than about 1 \AA were tentatively identified as Ly α for a metal line system. The resulting redshift was used as a trial redshift and the matches with

metal lines were noted and critiqued as above.

A metal line system identification is considered a strong one if it is corroborated by a spectrum from the literature that extends redward of Ly α emission. A system is considered reasonable if it consists of at least the minimum number of lines and the strengths of those lines are in agreement with the expected f values and range in doublet ratios.

An identification is marked as a possible identification if either the doublet ratio gives a value less than one or greater than two, ie. one of the doublet lines is a blend if it is present, or if the separation between that line and another line in the redshift system (excluding doublet pairs) is greater than $\sim 200 \text{ km s}^{-1}$ but less than $\sim 300 \text{ km s}^{-1}$. Once metal lines were identified, they were removed from the line list used for the Ly α forest analysis. Also, the redshift path covered by each line was removed from the analysis by removing a region of width 2.5σ centered on the wavelength centroid of the line. The line σ and line centroid were taken from the Gaussian fit.

The redshift of any spurious line in our 3σ line lists identified as a metal line would also have to match with other metal lines in our line list, specifically to a strong Lyman α line if it is observable in the spectrum. For this reason, we expect that the possible low occurrence of false lines of less than 5σ significance in our line lists has no effect on the metal line systems identified below.

3. NOTES ON INDIVIDUAL OBJECTS

3.1. *Q 0006+020* $z_{em} = 2.340$

This QSO was identified by Foltz et al. (1989). Tytler et al. (1993), hereafter T93, discuss the redshift systems they find in their red ($4312 \text{ \AA} - 7059 \text{ \AA}$), low resolution (8.6 \AA FWHM) spectrum of this object. We do not confirm the first system they find at $z_{abs} = 1.131$. This identification was based on the detection of Mg II $\lambda \lambda 2796, 2803$ at 5960 \AA and 5975 \AA respectively which we do not detect in our red spectrum of this object, which is presented in Paper II of this series. The second system T93 find is at $z_{abs} = 2.034$ for which they identify the C IV doublet at 4700 \AA and Al II $\lambda 1670$ at 5073 \AA . The positions of Ly α and Si III $\lambda 1206$ for this redshift lie on bad columns in the data, but we identify N II $\lambda 1083$ at 3289 \AA , a possible N V doublet at 3757 \AA and 3770 \AA , Si II $\lambda 1260$ at 3825 \AA , and C II $\lambda 1334$ at 4050 \AA . In addition, our red spectrum of this QSO confirms the C IV doublet and Al II identifications of T93 while also revealing the Si IV doublet at 4227 \AA and 4252 \AA and a possible Si II $\lambda 1526$ line at 4632 \AA . Identifying the 4700 \AA line in the spectrum of T93 as Si IV $\lambda 1393$ reveals the third system, at $z_{abs} = 2.374$. We identify Ly β at 3460 \AA , O VI $\lambda 1031$ and $\lambda 1037$ at 3482 \AA and 3501 \AA , and N I $\lambda 1200$ at 4050 \AA . Our red data confirm the 4700 \AA feature as well as the C IV doublet at $\sim 5222 \text{ \AA}$ for this redshift. This system is consistent with an associated absorber as proposed by Foltz et al. (1989).

We also detect several other systems using the methods and criteria described above:

$z_{abs} = 1.6094$ - This is a system showing Si II $\lambda 1260$ at 3289 \AA , C II $\lambda 1334$ at 3482 \AA , Si IV $\lambda 1393$ at 3637 \AA (the position of the $\lambda 1402$ component lies on a bad column but there is an absorption feature at this wavelength in our red spectrum), and Si II $\lambda 1526$ at 3984 \AA (which is blended

with Ly α at $z_{abs} = 2.2775$.) In addition, our red spectrum (see Paper II) shows a line at 4362 Å, consistent with Al II λ 1670 for this redshift.

$z_{abs} = 1.8189$ - At this redshift, we identify Ly α at 3427 Å, N I λ 1200 at 3383 Å, a tentative N V doublet at 3491 Å and 3501 Å (where the λ 1242 component must be blended with Ly α at $z_{abs} = 1.880$ and/or O VI λ 1037 at $z_{abs} = 2.375$), and C II λ 1334 at 3762 Å. The C IV doublet at this redshift is visible in our red spectrum at a wavelength of 4367 Å.

$z_{abs} = 1.8409$ - For this system, we detect Ly α 3454 Å, Si III λ 1206 at 3427 Å, Si II λ 1260 at 3579 Å, and C II λ 1334 at 3791 Å. Our red spectrum does not show any lines redward of Ly α consistent with this redshift.

$z_{abs} = 1.8802$ - This system is composed of Ly α at 3501 Å, a N V doublet at 3568 Å and 3579 Å, C II λ 1334 at 3845 Å, and a possible weak Si IV λ 1393 line at 4015 Å (no λ 1402 is detected.) No lines redward of Ly α emission are detected in the red spectrum.

$z_{abs} = 2.2775$ - This is a system showing Ly α at 3984 Å, Ly β at 3363 Å, Si III λ 1206 at 3955 Å, and the N V doublet at 4060 Å and 4072 Å. (The position of Fe II λ 1145 falls on a bad column for this redshift.) A possible C IV doublet identification is made from the red spectrum at 5076 Å.

Lastly, we find a possible Mg II absorber at $z_{abs} = 0.448$. However, the implied Fe II lines are not consistent with line ratios. Therefore, since only two lines are found, this system cannot qualify as a metal line system by our criteria.

3.2. *Q 0027+014* $z_{em} = 2.310$

Steidel & Sargent (1992), hereafter SS92, find a single Mg II system for this object at $z_{abs} = 1.2664$ using their red setup (5128-8947 Å) with 4-6 Å resolution. In addition to Mg II λ 2796, 2803 (at 6336 Å and 6352 Å respectively), they identify Fe II λ 2382 at 5400 Å. We confirm this system with our detection of the C IV doublet at 3508 Å and 3513 Å as well as Al II λ 1670 at 3786 Å. Our red spectrum of this object (see Paper II) shows the Fe II line found by SS92, but shows only marginal evidence for the Mg II doublet.

We also identify two other redshift systems in our spectrum:

$z_{abs} = 1.8415$ - We find Ly α at 3454 Å, N I λ 1200 at 3411 Å, Si III λ 1206 at 3428 Å, Si II λ 1260 at 3582 Å, a possible, blended C II λ 1334 line 3793 Å, and the Si IV doublet at 3960 Å and 3986 Å. However, the doublet ratio for the Si IV doublet is greater than two; therefore, the λ 1393 component must be blended. Our red spectrum shows Si II λ 1526 at 4337 Å, the C IV doublet at 4403 Å, Fe II λ 1608 at 4572 Å, and Al II λ 1670 at 4748 Å.

$z_{abs} = 1.9859$ - Ly α for this possible system is found at 3630 Å. At this redshift, we also identify N II λ 1083, Fe II λ 1145, Si II λ 1193 and λ 1260 lines at 3237 Å, 3419 Å, 3563 Å, and 3763 Å. The equivalent widths relative to Ly α indicate each of these must be blended. A Si III λ 1206 line is found at 3603 Å. The red spectrum shows no lines for this redshift redward of Ly α emission.

3.3. *Q 0037-018* $z_{em} = 2.341$

Wolfe et al. (1986), hereafter W86, find a candidate damped Ly α system present in the spectrum of this ob-

ject at 3602 Å ($z_{abs} = 1.962$) with an observed equivalent width of 15.5 Å. They also note an absorption feature at 3832 Å ($z_{abs} = 2.152$). However, since their objective was to search for and characterize damped Ly α systems only, they do not produce detailed line lists for their spectra. These lines are not confirmed by our data. We find no significant absorption feature at 3602 Å; but we do find a line at 3604 Å. We also find no significant line at 3832 Å. Due to the low signal-to-noise at the blue end of our spectrum, we truncated the spectrum for the purposes of our line searches. The usable portion of our spectrum therefore extends from ~ 3542 Å to ~ 4110 Å. The features at 3998 Å, 4003 Å, 4007 Å, and 4011 Å are identified as traps in the CCD, as they appear in many other object spectra.

3.4. *Q 0049+007* $z_{em} = 2.279$

We find a system consistent with Ly α at 3540 Å. SS92 (cf. Section 3.2) identify this metal line system at $z_{abs} = 1.9115$ on the basis of weak Al III λ 1854 and λ 1862 lines and a weak Mg II doublet. Further corroboration of this system comes from a possible N V λ 1238 line at 3607 Å (no λ 1242 is detected) and the Si IV doublet at 4057 Å and 4084 Å respectively in our data. Our red spectrum of this object (see Paper II) also shows Si II λ 1526 at 4445 Å, and the C IV doublet at 4507 Å and 4515 Å, consistent with this system.

In addition, we find five other systems or possible systems from our data:

$z_{abs} = 1.3865$ - We identify this system based on the C IV doublet at 3695 Å and 3701 Å. We also find Si II λ 1526 at 3643 Å, and Al II λ 1670 at 3987 Å. SS92 do not find a Mg II doublet nor do they find any Fe II lines at this redshift. Our red spectrum shows possible Al III λ 1854 and λ 1862 lines at 4426 Å and 4445 Å. However, the feature at 4445 Å is more likely Si IV λ 1393 at $z_{abs} = 2.1908$.

$z_{abs} = 1.5226$ - This system is composed of O I λ 1302 at 3285 Å, Si IV λ 1393 at 3515 Å and λ 1402 at 3540 Å (blended with Ly α at $z_{abs} = 1.9123$), a possible identification of Si II λ 1526 at 3850 Å, and the C IV doublet at 3905 Å and 3912 Å. SS92 do not detect a Mg II doublet or any Fe II lines at this redshift, nor do we find any matching lines in our red spectrum.

$z_{abs} = 2.1168$ - This is a relatively insecure identification based upon Ly α at 3789 Å, a possible O I λ 1302 at 4057 Å and possible Si II λ 1193 and λ 1260 lines at 3720 Å and 3927 Å. No lines are found redward of Ly α emission.

$z_{abs} = 2.1667$ - This system shows Ly α at 3850 Å, Ly β at 3248 Å, and a very tentative N V doublet both components of which must be blends at 3927 Å and 3935 Å. We find no lines at this redshift in our red spectrum

$z_{abs} = 2.1918$ - For this system, we find Ly α at 3880 Å, Ly β at 3274 Å, Si III λ 1206 at 3850 Å, and a possible, blended N II λ 1083 at 3458 Å. In addition, our red spectrum shows the Si IV doublet at 4447 Å and 4476 Å and the C IV doublet at 4944 Å.

3.5. *Q 0123+257* $z_{em} = 2.370$

The absorption spectrum of this QSO has been observed by Schmidt & Olsen (1968) (SO68), Oemler & Lynds (1975) (OL75), and W86 (cf. Section 3.3).

We confirm the absorption features seen by SO68 at 3900 Å, 4013 Å, 4057 Å, and 4065 Å. The remainder of

their features lie outside the wavelength range of our spectrum. They report an absorption system at $z_{abs} = 2.3683$, an associated absorber, from the identification of Ly α and the C IV doublet, as well as a possible identification of Si III $\lambda 1206$. OL75 discuss several possible redshift systems. The only system they find compelling, however, is the $z_{abs} = 2.3683$ system of SO68. We confirm several lines possibly associated with this system: Ly β at 3456 Å, O VI $\lambda\lambda 1031, 1037$ at 3473 Å and 3496 Å, N II $\lambda 1083$ at 3645 Å, and Si III $\lambda 1206$ at 4064 Å which is blended with Ly α at $z_{abs} = 2.3433$. Our red spectrum of this object (see Paper II) shows the C IV doublet at 5216 Å and 5226 Å. We also confirm the absence of any marked damped Ly α absorption, as reported by W86.

We tested all of the possible redshift systems proposed by OL75 and used our usual methods for finding additional metal line systems. As a result, we identify three other systems:

$z_{abs} = 0.3207$ - This system consists of Fe II $\lambda 2600$ at 3433 Å, a Mg II doublet at 3693 Å and 3702 Å, and Mg I $\lambda 2753$ at 3767 Å.

$z_{abs} = 1.8427$ - This system consists of Ly α at 3456 Å, Si III $\lambda 1206$ at 3430 Å, O I $\lambda 1302$ at 3702 Å, and Si IV $\lambda 1393$ at 3962 Å, with a possible identification of $\lambda 1402$ blended with a feature at 3989 Å.

$z_{abs} = 2.0379$ - For this system, we find Ly α at 3693 Å, Fe II $\lambda 1143$ and a blended $\lambda 1145$ at 3473 Å and 3478 Å, and N I $\lambda 1200$ at 3645 Å. Neither SO68 nor OL75 note any absorption features at the position of Fe II $\lambda 1608$ for this redshift; and our red spectrum shows no lines at this redshift.

3.6. Q 0150-203 $z_{em} = 2.148$

The absorption spectrum of 0150-203 (UM675) is first discussed in detail by Sargent et al. (1988), hereafter SBS88. Their data provide coverage from 3815 Å to 5038 Å with 1.5 Å resolution. They report several absorption systems from their spectrum:

$z_{abs} = 0.3892$ - A Mg II doublet is identified at this redshift. SBS88 report the possible blending of the Mg II doublet at $z_{abs} = 0.3892$ with a second component at $z_{abs} = 0.3882$. Our spectrum does show two prominent absorption features at 3883 and 3896 Å. If these lines are interpreted as the Mg II doublet the resulting redshifts are $z_{abs} = 0.38869$ for the $\lambda 2796$ line and $z_{abs} = 0.38977$ for the $\lambda 2803$ line, an unacceptable separation of 233 km s⁻¹. It is possible to identify three Fe II lines at this redshift, $\lambda 2344$ at 3253 Å, $\lambda 2382$ at 3308 Å, and $\lambda 2586$ at 3590 Å. However, no Fe II $\lambda 2600$ line is found which calls the identification of the $\lambda 2344$ and the $\lambda 2586$ lines into question. Given these arguments and the more compelling identification of the 3883 Å and 3896 Å features as the N V doublet at $z_{abs} = 2.134$, we consider this system improbable.

$z_{abs} = 0.7800$ - A Mg II system showing Fe II $\lambda 2382$ is reported by SBS88. The only lines in our search list that fall within the wavelength range of our data for $z_{abs} = 0.7800$ are Al III $\lambda 1854$ and $\lambda 1862$, but we detect neither of these, and thus cannot confirm this system.

$z_{abs} = 1.7666$ - SBS88 detect a weak C IV doublet at this redshift. We confirm this system from our detection of Ly α at 3363 Å and possible identifications of O I $\lambda 1302$ at 3604 Å, and C II $\lambda 1334$ at 3693 Å.

$z_{abs} = 1.9287$ - SBS88 regard this weak C IV doublet as a probable system. We confirm this system through our identifications of Ly α at 3560 Å and tentative Si II $\lambda 1193$, $\lambda 1260$, and $\lambda 1304$ lines at 3494 Å, 3690 Å and 3821 Å respectively.

$z_{abs} = 2.0083, 2.0097$ - SBS88 regard this C IV complex as almost certain due to the good redshift agreement between the putative doublet lines. The Si IV $\lambda 1393$ line is also identified for the $z_{abs} = 2.0097$ component of this complex. We confirm the $z_{abs} = 2.0083$ system. At this redshift, we identify lines of Ly α at 3657 Å, Fe II $\lambda 1145$ at 3444 Å, Si II $\lambda 1193$ at 3590 Å (possible), Si II $\lambda 1260$ at 3792 Å, N V $\lambda 1238$ at 3726 Å (possible), and C II $\lambda 1334$ at 4014 Å. York et al. (1991) give this component a B rating, as SBS88 only identified the C IV doublet. For the $z_{abs} = 2.0097$ component, we confirm Ly α absorption at 3659 Å, or $z_{abs} = 2.0101$. We also find Fe II $\lambda 1145$ at 3446 Å, Si III $\lambda 1206$ at 3632 Å, and O I $\lambda 1302$ at 3918 Å. York et al. (1991) assign this system an A rating since SBS88 identified both C IV and Si IV $\lambda 1393$ at this redshift. In our spectrum, the Ly α lines for the components of this complex are within 5 Å of a third line, which, if identified as Ly α as well, gives $z_{abs} = 2.0060$. However, we detect only one other line (Si II $\lambda 1260$ at 3788 Å) for this redshift. This, and the fact that SBS88 find no C IV at $z_{abs} = 2.0060$ lead us to regard this additional identification as extremely uncertain.

SS92 (cf. Section 3.2) find no Mg II systems in their spectrum of this object although they note that for the SBS88 systems at $z_{abs} = 1.7666$, 1.9287, 2.0083, and 2.0097, these lines would have been visible in their spectrum if present. In fact, SS92 find no absorption features in their spectrum at all.

Beaver et al. (1991), hereafter B91, observed the far-UV spectrum of this object using the FOS on HST. The spectra range from 1630 Å to 2428 Å and were taken using two different apertures each resulting in ~ 8.0 Å resolution. In addition, optical spectra were obtained with the Lick telescope. These spectra cover 3250-6350 Å at 15 Å resolution and 3540-4120 Å at 1.8 Å resolution. B91 confirm the $z_{abs} = 0.7800$ system of SBS88 with their identification of Ly α at 2161 Å and Ly β at 1836 Å as well as their tentative identifications of C II $\lambda 1334$ at 2370 Å, and Si III $\lambda 1206$ at 2148 Å and their possible identification of C III $\lambda 977$ at 1736 Å. They also report one other system:

$z_{abs} = 2.1348$ - The optical spectra of B91 show strong absorption at 3810 Å which is identified as Ly α . This identification results in the coincidence of the N V doublet at this redshift with the Mg II doublet at $z_{abs} = 0.3892$ identified by SBS88. This system is corroborated by the tentative identification of Ne VIII $\lambda 770$ at 2417 Å and the uncertain identification of He I $\lambda 584$ at 1836 Å. We identify several lines for this associated absorber, including Ly α at 3810 Å, O VI $\lambda\lambda 1031, 1037$ at 3234 Å and 3253 Å, N II $\lambda 1083$ at 3397 Å, and N V $\lambda\lambda 1238, 1242$ at 3883 Å and 3896 Å. Also, as noted by B91, the spectrum of SBS88 shows some absorption near the position of the C IV doublet at this redshift (~ 4860 Å) but they do not identify this feature.

We identify one additional system in our data:

$z_{abs} = 0.3628$ - This system consists of Fe II $\lambda 2382$, $\lambda 2586$, and $\lambda 2600$ at 3249 Å, 3525 Å, and 3542 Å respec-

tively, as well as Mg II $\lambda\lambda 2796, 2803$ at 3810 \AA and 3821 \AA . B91 do not detect Ly α for this system in their FOS spectrum, however, its position at 1657 \AA would place it at the blue edge of their data where the signal-to-noise ratio is poor.

3.7. *Q 0153+744* $z_{em} = 2.341$

According to our searches, there is no previously published spectrum of this QSO. In our spectrum, we find only one possible metal line system, an associated absorber at $z_{abs} = 2.3456$. We consider this identification tentative, however, due to the fact that the Ly β line for this system is separated from the position of Ly α by 6σ . The other species detected are O VI $\lambda 1031$ and $\lambda 1037$ at 3453 \AA and 3472 \AA , Fe II $\lambda 1143$ and Fe II $\lambda 1145$ at 3826 \AA and 3831 \AA , and Si III $\lambda 1206$ at 4037 \AA . In addition, our red spectrum (see Paper II) does show a possible C IV doublet at 5179 \AA and 5188 \AA , but the doublet ratio is less than one.

3.8. *Q 0226-038* $z_{em} = 2.073$

The absorption line spectrum of this QSO has been studied by many authors. The first such investigation was undertaken by Carswell et al. (1976) using spectrograms spanning a wavelength range from 3200 \AA to 6000 \AA . Young, Sargent, and Boksenberg (1982b), YSB82 hereafter, obtained spectra from 3530 \AA to 5070 \AA with 2.2 \AA resolution. In addition, Lanzetta, Turnshek, & Wolfe (1987), LTW87 hereafter, obtained spectra from 6271 \AA to 8766 \AA with 4.5 \AA resolution and a signal-to-noise ratio between 18 and 32. This object was also observed by SS92 with their red setup and by SBS88 (cf. Section 3.2 and Section 3.6).

The spectrum we obtained for this object is, unfortunately, riddled with bad columns from the CCD. Therefore, we find no absorption systems from our data alone; instead, we use our spectrum to attempt to confirm the systems found by other authors:

$z_{abs} = 1.3284$ - SS92 confirm the Mg II identification for this system which was found by LTW87. SS92 also identify Fe II $\lambda 2344$, $\lambda 2382$, and $\lambda 2600$ in their red spectrum. They further corroborate this system by noting that lines found by YSB82 at 3606 \AA and 3611 \AA can be identified as the C IV doublet and that an unidentified line found by SBS88 at 3890 \AA can be identified as Al II $\lambda 1670$. Our data show the C IV $\lambda 1548$ line at 3604 \AA , but we find only a weak feature at the expected position of $\lambda 1550$. The position of Al II $\lambda 1670$ falls on a bad column in our data. There is a feature at 3555 \AA , the expected position of Si II $\lambda 1526$; but it is not identified as a significant line as it falls on another of the many bad columns.

$z_{abs} = 1.3558$ - YSB82 propose the identification of two lines, at 3647 \AA and 3654 \AA , in the Lyman α forest region of their spectrum with the C IV doublet at this redshift. We confirm the presence of these lines; however, given the lack of any other lines to strengthen this identification, the does not meet our criteria for a true metal line system.

$z_{abs} = 2.0435$ - SBS88 identify this system based on the identification of the Si IV and C IV doublets. The expected position of Ly α for this redshift falls on a bad column in our data; and we find only one other possible line for this redshift, Si III $\lambda 1206$ at 3672 \AA .

We do not confirm the absorption line at 3703 \AA re-

ported by Carswell et al. (1976)

3.9. *Q 0348+061* $z_{em} = 2.056$

SBS88 (cf. Section 3.6) find several absorption systems in their spectrum of this QSO ($3880 \text{ \AA} - 5060 \text{ \AA}$):

$z_{abs} = 0.3997$ - This system is a single Mg II doublet according to SBS88. We find only marginal evidence for a Mg II doublet at 3912 \AA and 3921 \AA from our red spectrum of this object (see Paper II).

$z_{abs} = 1.7975$ - SBS88 find a C IV doublet at this redshift. We verify Ly α absorption at 3400 \AA ; we detect a possible Si III $\lambda 1206$ line at 3374 \AA ; and our red spectrum shows the C IV doublet identified by SBS88 at 4328 \AA and 4336 \AA .

$z_{abs} = 1.8409$ - SBS88 find another C IV doublet at this redshift. We detect Ly α absorption at 3453 \AA , in agreement with this system. A possible Si II $\lambda 1260$ line at 3581 \AA is found for this redshift; and our red spectrum corroborates the C IV doublet found by SBS88 as well as showing Si IV $\lambda 1393$ at 3958 \AA (but no $\lambda 1402$) and a possible Si II $\lambda 1526$ line at 4335 \AA .

$z_{abs} = 1.9681$ - SBS88 find a C IV doublet along with C II $\lambda 1334$ and a possible Si IV $\lambda 1393$ line at this redshift. We find Ly α 3608 \AA , Si III $\lambda 1206$ at 3581 \AA , and a very tentative N V doublet at 3676 \AA and 3687 \AA , which, if present, is highly blended with Ly α at $z_{abs} = 2.0238$ and $z_{abs} = 2.0331$. Our red spectrum verifies the identifications of SBS88 listed above and also shows Fe II $\lambda 1608$ at 4775 \AA .

$z_{abs} = 2.0237$ - SBS88 find a C IV doublet and possible Si IV $\lambda 1393$ at this redshift. SS92 (cf. Section 3.2) confirm this system in their red spectrum ($5128 \text{ \AA} - 8947 \text{ \AA}$) of this object with the detection of a Mg II doublet at this redshift. They do not detect Mg II for any of the other SBS88 redshifts to which their spectrum is sensitive ($z_{abs} > 0.83$.) We detect Ly α absorption at 3676 \AA , in agreement with this system. In addition, we identify a possible blended Si II $\lambda 1193$ line at 3608 \AA , N I $\lambda 1200$ at 3628 \AA , Si III $\lambda 1206$ at 3648 \AA , Si II $\lambda 1260$ at 3812 \AA , and C II $\lambda 1334$ at 4035 \AA . Our red spectrum exhibits the features found by SBS88 listed above as well as C II $\lambda 1334$ at 4037 \AA .

$z_{abs} = 2.0330$ - SBS88 identify both C IV and Si IV doublets for this redshift. We detect Ly α at 3687 \AA and Si III $\lambda 1206$ at 3659 \AA . Our red spectrum shows marginal evidence for the features listed by SBS88.

3.10. *Q 0400+258* $z_{em} = 2.108$

No previously published absorption line spectrum of this QSO was found in our searches. Unfortunately, the low signal-to-noise of the blue portion of our spectrum ($3208 \text{ \AA} - 3659 \text{ \AA}$) prevents us from identifying any lines in the Lyman alpha forest. We find only one significant line at 3752 \AA from which we cannot identify any metal line systems.

3.11. *Q 0747+610* $z_{em} = 2.491$

In their catalog of QSO absorption lines, Junkkarinen et al. (1991) note two metal line systems found for this object by Afanasjev et al. (1979). These systems were identified at $z_{abs} = 1.986$ and $z_{abs} = 2.210$. York et al. (1991) give both of these systems a B rating in their reference catalog of heavy element systems in QSO spectra.

According to their explanation of their rating system, this B rating indicates that either a C IV or Mg II doublet was identified for these systems with the correct doublet ratio, but that no other lines but Lyman alpha were detected. However, Junkkarinen et al. note that for the $z_{abs} = 1.986$ system, N V, Si II, C II, Si IV, and Al II lines were detected in addition to H I and C IV; and for the $z_{abs} = 2.210$ system, Si II*, N V, C II, Si IV, and Al III lines were detected in addition to H I and C IV. SS92 (cf. Section 3.2) do not confirm either of these metal line system redshifts. Instead, they find three others at $z_{abs} = 1.1282$, $z_{abs} = 2.0076$, and $z_{abs} = 2.4865$.

We confirm the $z_{abs} = 1.986$ system of Afanasjev et al. (1979) with our identification of Ly α at 3629 Å, a possible N I λ 1135 at 3389 Å, a possible Si II λ 1190 line at 3554 Å, Si II λ 1193 at 3562 Å, and N I λ 1200 at 3582 Å. We also confirm their $z_{abs} = 2.210$ system with our detection of Ly α at 3903 Å, a possible N II λ 1083 line at 3480 Å, Si III λ 1206 at 3874 Å, Si II λ 1260 at 4047 Å, and O I λ 1302 at 4180 Å.

We do not find any lines at the position of the $z_{abs} = 1.1282$ system of SS92 which they identify by a weak Mg II doublet. We identify a metal line system at $z_{abs} = 2.0071$, in accordance with the $z_{abs} = 2.0076$ system found by these authors. At this redshift, we find a strong Ly α line at 3656 Å, Si II λ 1190 and λ 1193 at 3580 Å and 3589 Å, Si III λ 1206 at 3629 Å, Si II λ 1260 and λ 1304 at 3791 Å and 3923 Å, O I λ 1302 at 3915 Å, and possible C II λ 1334 absorption at 4014 Å. It is clear that some of these Si II lines are blends given their relative strengths. Our confirmation of the $z_{abs} = 2.4865$ system of SS92 is not as strong. We find Ly α and Ly β at 4237 Å and 3575 Å respectively for this redshift. But we do not detect any other species with any confidence.

The absorption line spectrum of this object is a rich one. We find a total of 145 significant lines and we find twelve metal line systems in addition to the ones discussed above. As is the case for all of our objects, it is unlikely that all of these systems are real since SS92 do not report any lines from their red spectrum at these redshifts. However, we have kept all the systems that cannot be definitively ruled out on the basis of our data. For all redshifts below 1.742, the Ly α line falls outside the spectral range of our data. The values of these redshifts are based upon the strongest line that was detected for each system.

$z_{abs} = 1.4102$ - This system is based upon a C IV doublet at 3731 Å and 3738 Å and a Si IV doublet at 3359 Å and 3381 Å. We also find Al II λ 1670 at 4028 Å.

$z_{abs} = 1.4529$ - The value for this redshift is based upon a C IV doublet at 3798 Å and 3804 Å. In addition, we detect Si IV λ 1393 at 3419 Å and Si IV λ 1402 at 3441 Å (though it must be a blend if it is present otherwise the Si IV doublet ratio is less than one), Si II λ 1526 at 3745 Å, and Al II λ 1670 at 4098 Å.

$z_{abs} = 1.5986$ - For this system, we identify Si II λ 1304 at 3389 Å, possible C II λ 1334 absorption at 3466 Å, a possible Si IV λ 1393 line at 3621 Å (no λ 1402 is found), Si II λ 1526 at 3967 Å, and a possible, weak C IV λ 1548 line at 4023 Å. A weak feature is present at the position of C IV λ 1550, but it is not identified as a significant (3σ) line.

$z_{abs} = 1.6822$ - This redshift is based upon Si II λ 1260.

We also find a possible blended N V λ 1242 line at 3333 Å (λ 1238 is out of the wavelength range of our line list), O I λ 1302 at 3492 Å, Si II λ 1304 at 3498 Å, C II λ 1334 at 3580 Å, and a rather doubtful Si IV doublet at 3738 Å and 3761 Å.

$z_{abs} = 1.7324$ - This system, based on a possible C IV doublet at 4230 Å and 4237 Å, is a relatively tentative one due to the inconsistent doublet ratios of this pair and of a possible Si IV doublet at 3808 Å and 3833 Å. We also find O I λ 1302 at 3558 Å.

$z_{abs} = 1.8123$ - For this system, we find Ly α at 3419 Å. In addition, we find a possible Si II λ 1193 line at 3357 Å, Si III λ 1206 at 3393 Å, a possible blended Si II λ 1260 line at 3544 Å, O I λ 1302 at 3662 Å, and C II λ 1334 at 3753 Å.

$z_{abs} = 1.8728$ - This system consists of Ly α at 3492 Å, Si II λ 1190 and λ 1193 at 3419 Å and 3428 Å, N I λ 1200 at 3447 Å, Si III λ 1206 at 3466 Å, a possible N V λ 1238 line at 3558 Å, Si II λ 1260 at 3621 Å, C II λ 1334 at 3833 Å and a possible Si IV λ 1393 at 4003 Å (no λ 1402 component is found.)

$z_{abs} = 2.0070, 2.0093$ - We find a metal line system of two components at these redshifts. The first component shows Ly α at 3656 Å, Si II λ 1190 and λ 1193 at 3580 Å and 3589 Å, a possible Si III λ 1206 line at 3618 Å, Si II λ 1260 and λ 1304 at 3791 Å and 3923 Å, C II λ 1334 at 4014 Å, and Si IV λ 1393 at 4192 Å. The λ 1402 component of this doublet is blended with the same line corresponding to the other system at $z_{abs} = 2.009$. The second component consists of Ly α at 3658 Å, a possible N V λ 1238 line at 3728 Å (no λ 1242 line is found), Si II λ 1260 at 3792 Å, C II λ 1334 at 4015 Å, and a tentative Si IV doublet at 4194 Å and 4221 Å (with a doublet ratio less than one due to blending.)

$z_{abs} = 2.0476$ - This system is composed of Ly α at 3705 Å, N I λ 1200 at 3656 Å (blended with Ly α at $z_{abs} = 2.007$ if present), Si III λ 1206 at 3677 Å, O I λ 1302 at 3967 Å, and Si IV λ 1393 at 4247 Å.

$z_{abs} = 2.1391$ - At this redshift, we identify Ly α at 3816 Å, N I λ 1135 and λ 1200 at 3562 Å and 3767 Å, and a possible N V doublet at 3889 Å and 3901 Å for which the λ 1242 component must be blended as it is stronger than both the λ 1238 component of the doublet and Ly α .

$z_{abs} = 2.1724$ - This system consists of Ly α at 3856 Å, tentative N I λ 1135 and λ 1200 lines at 3601 Å and 3808 Å, Si III λ 1206 at 3828 Å, and a possible C II λ 1334 line at 4235 Å.

$z_{abs} = 2.2849$ - This system is identified on the basis of strong Ly α absorption at 3993 Å, Ly β at 3369 Å, O VI λ 1031 and λ 1037 at 3389 Å and 3408 Å, possible Si II λ 1190 and λ 1193 lines at 3777 Å and 3786 Å, and a possible Si III λ 1206 line at 3964 Å.

3.12. *Q 0836 + 710* $z_{em} = 2.218$

Stickel & Kühr (1993) report an absorption feature in their spectrum of this object at 5360 Å which they identify as the Mg II doublet at $z_{abs} = 0.914$. We find Al III λ 1854 at 3550 Å. Also, we have a red spectrum of this object in the vicinity of Mg II emission. This spectrum does show the Mg II doublet at 5359 Å and 5372 Å, giving a redshift of 0.916.

We find several other redshift systems in our data:

$z_{abs} = 1.4256$ - This system is a double-component C IV

absorber with the Si IV doublet at 3380 Å and 3403 Å, the C IV doublet at 3755 Å and 3762 Å, a possible Si II λ1526 at 3702 Å, and Fe II λ1608 at 3902 Å. Two components in each line are evident in the spectrum, with the second, weaker component at $z_{abs} = 1.4249$ which, unlike the first component, shows Al II λ1670 absorption, at 4051 Å.

$z_{abs} = 1.6681$ - At this redshift, we detect absorption from Lyα at 3243 Å, C II λ1334 at 3561 Å, and a Si IV doublet at 3719 Å and 3742 Å (though its implied doublet ratio is less than one.) There is no Mg II absorption in our red spectrum.

$z_{abs} = 1.7331$ - This system consists of Lyα at 3322 Å, O I λ1302 at 3558 Å, the N V doublet at 3386 Å and 3397 Å, and a possible Si IV λ1393 line at 3809 Å. The expected position of the Mg II doublet falls on a poorly subtracted sky line in the red spectrum.

We find a two-component associated absorption system at $z_{abs} = 2.1800$ consisting of only Lyα (3866 Å) and Lyβ (3261 Å and 3263 Å.)

The absorption features at 3964 Å, 3970 Å, 3975 Å, and 3983 Å are identified as traps in the CCD.

3.13. *Q 0848+153* $z_{em} = 2.014$

YSB82 (cf. Section 3.8) find eight absorption lines blueward of Lyα emission in their spectrum of this QSO. They do not identify any of them. SBS88 (cf. Section 3.6) detect only one line in their spectrum of this object (one which is not found by YSB88.) SS92 (cf. Section 3.2) find four absorption features in their red spectrum and identify three of them as a Mg II doublet and Fe II λ2600 at $z_{abs} = 1.0254$. Neither we nor YSB82 nor SBS88 observed the region of the spectrum necessary to confirm the C IV doublet for this system; but we do identify Fe II λ1608 at 3259 Å. We find no other lines at this redshift or any other metal line systems from our data. We do note that lines 8 and 11 in our line list match the position of the Si IV doublet at $z_{abs} = 1.5738$ well, although we cannot call this a true metal line system based on our criteria.

3.14. *Q 0936+368* $z_{em} = 2.025$

We have found no previously published spectrum of this object. Due to low signal-to-noise in the blue region of our spectrum (3200-3400 Å) the spectrum was truncated at roughly 3400 Å for the purposes of the line list. The absorption features at 3942 Å, 3948 Å, and 3955 Å are traps in the CCD.

The only system found is a C IV doublet at 4001 Å and 4006 Å and C II λ1334 at 3448 Å from a system at $z_{abs} = 1.5841$.

3.15. *Q 0952+335* $z_{em} = 2.504$

Our spectrum of this object shows a damped Lyman alpha system at 3765 Å with an observed equivalent width of 30.97 Å. The absorption features at 4277 Å, 4282 Å, 4286 Å, and 4290 Å are traps in the CCD. We find ten possible metal line systems:

$z_{abs} = 0.5393$ - This system consists of several Fe II lines (λ2344 at 3609 Å, λ2374 at 3655 Å, λ2382 at 3668 Å, λ2586 at 3981 Å, and λ2600 at 4002 Å) and a possible Mg II doublet at 4304 Å and 4314 Å. However, these Mg II lines are weaker than all of the Fe II lines identified, contrary to what is expected; and the relative strengths of

the Fe II lines are also not entirely consistent with the expected values. Although the possibility of blending keeps us from ruling out this system altogether, it is a tentative one.

$z_{abs} = 1.5362$ - This redshift is based upon a C IV λ1548 line at 3927 Å. The expected position of C IV λ1550 for this redshift falls on a bad column in the data. We also detect a Si IV doublet at 3535 Å and 3558 Å, Si II λ1526 at 3872 Å, Fe II λ1608 at 4079 Å, and Al II λ1670 at 4237 Å.

$z_{abs} = 2.0399$ - For this system, we find Lyα at 3695 Å, Si III λ1206 at 3668 Å, C II λ1334 at 4055 Å, and the Si IV doublet at 4237 Å and 4265 Å. Also, the position of the N V doublet falls within the damped Lyman alpha line at 3763 Å.

$z_{abs} = 2.0555$ - Lyα for this system is found at 3714 Å. We also identify Fe II λ1145 absorption at 3498 Å, possible Si III λ1206 absorption at 3687 Å, possible Si II λ1260 and λ1304 absorption at 3850 Å and 3985 Å, and a Si IV doublet at 4258 Å and 4286 Å.

$z_{abs} = 2.0965$ - This system is the damped Lyα absorber noted above. The metal lines found at this redshift include Si II λ1190 and λ1193 at 3685 Å and 3695 Å (possible), a N I λ1200 line at 3714 Å, Si III λ1206 at 3735 Å, Si II λ1260 at 3903 Å, C II λ1334 at 4130 Å, and Si IV λλ1393,1402 at 4314 Å and 4342 Å.

$z_{abs} = 2.1670$ - For this system, we find Lyα at 3850 Å, Fe II λ1143 and λ1145 at 3620 Å and 3626 Å, N I λ1200 at 3801 Å, and Si III λ1206 at 3820 Å.

$z_{abs} = 2.1850$ - This system consists of Lyα at 3872 Å, Si II λ1193 at 3801 Å, N I λ1200 at 3820 Å, Si II λ1260 and λ1304 at 4014 Å and 4153 Å, and O I λ1302 at 4147 Å.

$z_{abs} = 2.2102$ - At this redshift, we detect Lyα at 3903 Å, Si II λ1190 and λ1193 at 3820 Å and 3830 Å, Si III λ1206 at 3872 Å, a possible N V λ1238 line at 3976 Å (no λ1402 component is found), a blended Si II λ1260 line at 4046 Å, and O I λ1302 at 4180 Å. The expected position of Si II λ1304 falls on a bad column in the data.

$z_{abs} = 2.2924$ - For this system, we identify Lyα at 4002 Å, N II λ1083 at 3569 Å, Si III λ1206 at 3972 Å, and the N V doublet at 4079 Å and 4092 Å.

$z_{abs} = 2.3189$ - This system consists of Lyα at 4035 Å, Fe II λ1143 and λ1145 at 3795 Å and 3801 Å, Si II λ 1193 at 3959 Å, and Si II λ1260 at 4183 Å.

3.16. *Q 0955+472* $z_{em} = 2.482$

We note the presence of associated absorption in the spectrum of this radio loud QSO, at 4203 Å, 4206 Å, 4219 Å, and 4241 Å, separated from the position of the Lyman alpha emission by 2121 km s⁻¹, 1910 km s⁻¹, 990 km s⁻¹, and -539 km s⁻¹, respectively. We do not find metal line systems consistent with these redshifts, but we do find Lyβ absorption in our spectrum for the first, third, and fourth systems listed above at 3547 Å, 3561 Å, and 3579 Å. The Lyβ line for the second system appears to be blended with Lyβ for the first system at 3549 Å, but is not identified as a significant line by our line-finding program. The metal line systems we find are as follows:

$z_{abs} = 1.7251$ - This system is identified on the basis of a possible C IV doublet at 4219 Å and 4225 Å. The other metal lines detected are O I λ1302 at 3547 Å and Si II λ1304 at 3554 Å. This system is relatively insecure.

$z_{abs} = 2.2849$ - For this system, we find Ly α at 3993 Å, N II $\lambda 1083$ at 3561 Å, blended N I $\lambda 1200$ absorption at 3943 Å, Si III $\lambda 1206$ at 3963 Å, and a possible N V doublet for which the $\lambda 1238$ component is blended with the Lyman alpha complex at 4071 Å, and the $\lambda 1242$ component is detected at 4082 Å.

$z_{abs} = 2.3453, 2.3481$ - Ly α for this system is part of the Lyman alpha complex at 4067 Å. Other lines detected include a possible, blended N I $\lambda 1135$ line and N I $\lambda 1200$ at 3796 Å and 4014 Å, Fe II $\lambda 1145$ at 3830 Å, Si II $\lambda 1190$ and $\lambda 1193$ at 3984 Å and 3993 Å, Si III $\lambda 1206$ at 4038 Å, and a possible N V doublet at 4144 Å and 4156 Å.

$z_{abs} = 2.4087$ - This system consists of Ly α at 4144 Å, N I $\lambda 1135$ and $\lambda 1200$ at 3869 Å and 4090 Å, and Si III $\lambda 1206$ at 4112 Å. Despite the fact that the putative N I $\lambda 1135$ line shows good redshift agreement with this system, it is treated as a possible identification because the stronger line of the same species, N I $\lambda 1200$, shows poorer agreement.

The absorption features at 4277 Å, 4282 Å, 4286 Å, and 4290 Å are traps in the CCD.

3.17. *Q 0956+122* $z_{em} = 3.308$

Sargent et al. (1989) obtained a spectrum of this object with 4 Å resolution from 3150 Å to 4700 Å and 6 Å resolution from 4600 Å to 7000 Å. They find weak C IV systems at $z_{abs} = 2.9145$ and $z_{abs} = 3.2230$. We find only Ly α at $z_{abs} = 2.9156$. The system at $z_{abs} = 3.2230$ is identified as a Lyman limit system by Steidel (1990) from a higher resolution (~ 1.1 Å) spectrum. He identifies C IV and Si IV doublets, Si III $\lambda 1206$, C III $\lambda 977$ and several Lyman series lines. We confirm this system with our detection of Ly α at 5134 Å, N I $\lambda 1200$ at 5069 Å, and Si III $\lambda 1206$ at 5095 Å. Songaila & Cowie (1996) identify this system as a partial Lyman limit system at $z_{abs} = 3.2216$. Sargent et al. (1989) also find a Lyman limit system with no corresponding heavy element lines at $z_{abs} = 3.096$. We identify strong Ly α absorption at this redshift as well as a possible Si II $\lambda 1260$ line at 5162 Å. Both of these lines are found in the spectrum of Steidel (1990), but they are not attributed to a Lyman limit system. Instead, Steidel (1990) finds another Lyman limit system at $z_{abs} = 3.11$. We detect strong Lyman alpha absorption at this redshift as well as Si III $\lambda 1206$. The position of Si II $\lambda 1260$ falls on a trap in the CCD. Several other metal line systems were also found by this author:

$z_{abs} = 0.0456$ - Our spectrum does not extend far enough into the red to allow us to confirm the Na I $\lambda 5891$, 5897 lines tentatively identified at this redshift.

$z_{abs} = 2.3104$ - Steidel (1990) tentatively identifies Ly α , C IV $\lambda 1548$ and Al II $\lambda 1670$ at this redshift. We find C II $\lambda 1334$ at 4418 Å, a double-component Si IV doublet at 4614 Å and 4636 Å, Si II $\lambda 1526$ at 5054 Å, and C IV $\lambda 1548$ and $\lambda 1550$ (blended with Ly α at $z_{abs} = 3.223$) at 5125 Å and 5134 Å, Hu et al. (1995) identify this double-component Si IV doublet as well in a high resolution (~ 0.13 Å) spectrum taken with the HIRES Spectrograph on the Keck Telescope. The $\lambda 1393$ line is seen at $z_{abs} = 2.3104$ and $z_{abs} = 2.3109$.

$z_{abs} = 2.7169$ - Steidel (1990) finds C II $\lambda 1334$, a C IV doublet, and Al II $\lambda 1670$ at this redshift. We confirm this system with the detection of Ly α at 4519 Å, N I $\lambda 1200$ at

4461 Å, Si III $\lambda 1206$ at 4484 Å, the N V doublet at 4604 Å and 4618 Å, and C II $\lambda 1334$ at 4959 Å. The position of O I $\lambda 1302$ falls on a bad region in the spectrum.

$z_{abs} = 2.7261$ - Steidel (1990) finds a weak C IV doublet at this redshift. We do not find Ly α corresponding to this redshift.

$z_{abs} = 2.8320$ - Steidel (1990) finds a weak C IV doublet at this redshift as well as Ly β , Si II $\lambda 1260$, and C II $\lambda 1334$. We identify Ly α at 4659 Å, N I $\lambda 1200$ at 4599 Å, Si II $\lambda 1260$ at 4830 Å, a possible Si II $\lambda 1304$ line at 5002 Å (blended with Ly α at $z = 3.1145$), O I $\lambda 1302$ 4990 Å, and a possible C II $\lambda 1334$ line at 5118 Å.

$z_{abs} = 3.1045$ - Steidel (1990) identifies Ly α , C III $\lambda 977$, and the C IV doublet for this secure system. We confirm strong Ly α absorption at 4990 Å and find a Si II $\lambda 1260$ line at 5172 Å.

$z_{abs} = 3.1530$ - Steidel (1990) finds a weak C IV doublet, a Si IV doublet, Si II $\lambda 1190$ and $\lambda 1193$, Si III $\lambda 1206$, and several Lyman series lines. We detect Ly α at 5048 Å, a possible N I $\lambda 1200$ line at 4980 Å (blended with Ly α at $z_{abs} = 3.0963$), a tentative Si III $\lambda 1206$ line at 5012 Å, and the N V doublet at 5144 Å and 5157 Å. We detect the features identified by Steidel (1990) as Si II $\lambda 1190$ and $\lambda 1193$, but since our spectrum shows no feature at the position of Si II $\lambda 1260$, we do not confirm those identifications.

We identify several other possible metal line systems from our spectrum:

$z_{abs} = 2.8342$ - This system is separated by 172 km s⁻¹ from the system found by Steidel (1990) at $z_{abs} = 2.8320$. Ly α is detected at 4661 Å, the N V doublet at 4750 Å and 4765 Å, and Si II $\lambda 1260$ at 4832 Å. The Si II $\lambda 1304$ and C II $\lambda 1334$ identified with the $z_{abs} = 2.8320$ system are more likely associated with this system.

$z_{abs} = 3.0490$ - This system consists of Ly α at 4922 Å, possible Fe II $\lambda 1143$ and $\lambda 1145$ lines at 4630 Å and 4636 Å, Si III $\lambda 1206$ at 4884 Å and Si II $\lambda 1260$ at 5103 Å. Steidel (1990) finds no line which would correspond to Fe II $\lambda 1608$ at ~ 6510 Å or C IV at ~ 6270 Å.

$z_{abs} = 3.0528$ - At this redshift, we identify Ly α at 4927 Å, N I $\lambda 1135$ and $\lambda 1200$ at 4599 Å and 4862 Å, Si III $\lambda 1206$ at 4890 Å, and the N V doublet at 5021 Å and 5036 Å. There is a line in the Steidel (1990) line list at 6274 Å, which would correspond to C IV $\lambda 1548$ at this redshift, but none at 6285 Å, which would correspond to C IV $\lambda 1550$.

$z_{abs} = 3.1321$ - This system is composed of Ly α at 5023 Å, a possible N II $\lambda 1083$ line at 4480 Å, N I $\lambda 1135$ and $\lambda 1200$ at 4689 Å and 4959 Å, a possible N V doublet, both components of which are blended with other lines (see line list), at 5118 Å and 5134 Å, and Si II $\lambda 1260$ at 5208 Å. No C IV is detected by Steidel (1990).

$z_{abs} = 3.1975$ - At this redshift, we detect Ly α at 5103 Å, N I $\lambda 1200$ at 5036 Å, Si III $\lambda 1206$ at 5065 Å, and a possible N V doublet at 5200 Å and 5217 Å. A feature at 6497 Å in the line list of Steidel (1990) would correspond to C IV $\lambda 1548$ at this redshift, but no $\lambda 1550$ component is present.

$z_{abs} = 3.2461$ - This system consists of Ly α at 5162 Å, Fe II $\lambda 1143$ and $\lambda 1145$ at 4855 Å and 4862 Å, N I $\lambda 1135$ and $\lambda 1200$ at 4753 Å and 5095 Å, and Si III $\lambda 1206$ at 5122 Å. Steidel (1990) finds no C IV doublet or Fe II $\lambda 1608$ at this redshift.

$z_{abs} = 3.2774$ - At this redshift, we identify Ly α at 5200

\AA , N II $\lambda 1083$ at 4636 \AA , N I $\lambda 1135$ and $\lambda 1200$ at 4855 \AA and 5134 \AA , and Si III $\lambda 1206$ at 5162 \AA . Steidel (1990) finds no C IV at this redshift.

The absorption features at 5176 \AA , 5181 \AA , 5185 \AA , and 5189 \AA are identified as traps in the CCD.

3.18. *Q 1009+299* $z_{em} = 2.633$

There are no previously published absorption line spectra of this object. From our data, we find eight candidate metal line systems including a complex of associated absorption near the quasar redshift:

$z_{abs} = 1.8484$ - This system is identified by the C IV doublet at 4410 \AA and 4418 \AA , the $\lambda 1550$ component of which is blended with Ly α at $z_{abs} = 2.6339$. Other lines found include O I $\lambda 1302$ at 3709 \AA , Si II $\lambda 1304$ and $\lambda 1526$ at 3715 \AA and 4349 \AA .

$z_{abs} = 2.2611$ - For this system, we identify Ly α at 3964 \AA , Si III $\lambda 1206$ at 3934 \AA , Si II $\lambda 1260$ at 4110 \AA , O I $\lambda 1302$ at 4246 \AA , and a possible C II $\lambda 1334$ line at 4353 \AA . The expected positions of Fe II $\lambda 1143$ and $\lambda 1145$ fall on bad columns in the data.

$z_{abs} = 2.3582$ - This system is comprised of Ly α at 4082 \AA , N I $\lambda 1200$ at 4030 \AA , Si III $\lambda 1206$ at 4052 \AA , Si II $\lambda 1260$ at 4232 \AA , and O I $\lambda 1302$ at 4373 \AA .

$z_{abs} = 2.3809$ - At this redshift, we detect Ly α at 4110 \AA , N II $\lambda 1083$ at 3665 \AA , N I $\lambda 1200$ at 4056 \AA , Si III $\lambda 1206$ at 4079 \AA , a possible N V $\lambda 1242$ line at 4201 \AA (the expected position of the $\lambda 1238$ component falls on a bad region in the spectrum), and O I $\lambda 1302$ at 4403 \AA .

$z_{abs} = 2.4068$ - For this system, we identify very strong, weakly damped Ly α absorption at 4141 \AA , Si II $\lambda 1190$ at 4056 \AA (the position of Si II $\lambda 1193$ falls on a bad region in the spectrum), N I $\lambda 1200$ at 4087 \AA , Si III $\lambda 1206$ at 4110 \AA , Si II $\lambda 1260$ at 4294 \AA , and O I $\lambda 1302$ at 4436 \AA . The position of Si II $\lambda 1304$ falls on a bad column.

$z_{abs} = 2.5236$ - At this redshift, we identify Ly α at 4283 \AA , N I $\lambda 1135$ at 3998 \AA , Si II $\lambda 1193$ at 4205 \AA , N I $\lambda 1200$ at 4227 \AA , and Si III $\lambda 1206$ at 4252 \AA . The expected position of Si II $\lambda 1260$ falls on bad columns in the data.

$z_{abs} = 2.5531$ - This system consists of Ly α at 4319 \AA , Ly β at 3645 \AA , O VI $\lambda 1031$ and $\lambda 1037$ at 3667 \AA and 3686 \AA , N II $\lambda 1083$ at 3851 \AA , Fe II $\lambda 1143$ at 4061 \AA (the position of $\lambda 1145$ falls on bad columns in the spectrum), and Si II $\lambda 1193$ at 4240 \AA .

$z_{abs} = 2.6158$ - For this associated absorber, Ly α is found at 4396 \AA , Ly β at 3709 \AA , C II $\lambda 1036$ at 3746 \AA , possible Fe II $\lambda 1143$ and Fe II $\lambda 1145$ blended with Ly α at $z_{abs} = 2.40677$ at 4134 \AA and 4141 \AA , and Si III $\lambda 1206$ at 4362 \AA .

The absorption features at 4412 \AA , 4418 \AA , 4422 \AA , and 4425 \AA are identified as traps in the CCD.

3.19. *Q 1207+399* $z_{em} = 2.459$

According to our literature searches, there is no previously published absorption line spectrum of this QSO. From our data, we find two metal line systems:

$z_{abs} = 2.1116$ - At this redshift, we detect a blended Ly α line at 3781 \AA , Si III $\lambda 1206$ at 3765 \AA , Si II $\lambda 1260$ at 3922 \AA , C II $\lambda 1334$ at 4152 \AA , Si IV $\lambda \lambda 1393, 1402$ at 4337 \AA and 4365 \AA , and a possible C IV $\lambda 1548$ line at 4816 \AA . The expected position of C IV $\lambda 1550$ for this redshift falls just outside our spectral range.

$z_{abs} = 2.1561$ - At this redshift, we find Ly α at 3837 \AA , Ly β at 3238 \AA , Si III $\lambda 1206$ at 3808 \AA , the N V doublet at 3907 \AA and 3922 \AA , Si II $\lambda 1260$ at 3977 \AA , and C II $\lambda 1334$ at 4212 \AA .

The absorption features present at 4576 \AA , 4587 \AA , 4595 \AA and 4603 \AA are traps in the CCD.

3.20. *Q 1210+175* $z_{em} = 2.564$

This QSO was observed by Foltz et al. (1987) who noted a possible damped Lyman alpha system in their spectrum at roughly 3500 \AA . According to Wolfe et al. (1995) this system is a confirmed damped Ly α absorber with an equivalent width of 11.3 \AA . Ly α for this candidate is not within our spectral range for this object. However, we find five metal line systems from our data, one of which is consistent with this damped system.

$z_{abs} = 1.8917$ - This system is the damped Ly α absorber discussed above. Ly α at this redshift is outside our spectral range, but we do detect the Si IV doublet at 4030 \AA and 4056 \AA . Other lines detected include Si II $\lambda 1260$, $\lambda 1304$, and $\lambda 1526$ at 3645 \AA , 3772 \AA , and 4414 \AA , O I $\lambda 1302$ at 3765 \AA , and C II $\lambda 1334$ at 3859 \AA .

$z_{abs} = 2.0548$ - At this redshift, we identify Ly α at 3713 \AA , Si II $\lambda 1193$, $\lambda 1260$, and $\lambda 1304$ at 3645 \AA , 3850 \AA , and 3985 \AA , and C II $\lambda 1334$ at 4076 \AA . The Si II $\lambda 1304$ line must be a blend if it is present.

$z_{abs} = 2.1240$ - For this system, we detect Ly α at 3798 \AA , Si III $\lambda 1206$ at 3768 \AA , a N V doublet at 3868 \AA and 3881 \AA , a possible Si II $\lambda 1260$ line at 3938 \AA , and C II $\lambda 1334$ at 4169 \AA .

$z_{abs} = 2.1974$ - For this system, we identify Ly α at 3887 \AA , N I $\lambda 1200$ at 3837 \AA , Si III $\lambda 1206$ at 3859 \AA , Si II $\lambda 1260$ at 4030 \AA , O I $\lambda 1302$ at 4164 \AA , and C II $\lambda 1334$ at 4266 \AA .

$z_{abs} = 2.5786$ - This system consists of Ly α at 4350 \AA , Ly β at 3671 \AA , and O VI $\lambda 1031$ and $\lambda 1037$ at 3693 \AA and 3714 \AA . Both O VI lines are stronger than Ly α and Ly β indicating either that they are blends or that the line of sight through this absorber intersects regions dominated by highly ionized gas. The latter interpretation is likely because the redshift of this absorber is larger than the QSO emission redshift, indicating that this absorbing material must be infalling gas associated with the QSO itself.

3.21. *Q 1231+294* $z_{em} = 2.018$

Thompson et al. (1989) measure an emission redshift of $z_{em} = 2.011 \pm 0.001$ for this QSO from [O IV]+Si IV $\lambda \lambda 1397-1406$ and C III] $\lambda 1909$ emission lines. Our spectrum of Ly α emission gives a redshift of ~ 2.018 .

We find two metal line systems from our absorption line spectrum.

$z_{abs} = 1.4780$ - This system consists of the C IV doublet at 3836 \AA and 3843 \AA and the Si IV doublet at 3454 \AA and 3477 \AA .

$z_{abs} = 1.8755$ - For this system, we identify Ly α at 3496 \AA , possible N I $\lambda 1135$ and $\lambda 1200$ lines at 3264 \AA and 3450 \AA , a possible Fe II $\lambda 1145$ line at 3292 \AA , and O I $\lambda 1302$ at 3745 \AA , blended with C IV $\lambda 1550$ at $z_{abs} = 1.4145$.

Lastly, we identify a C IV doublet at $z_{abs} = 1.4145$ and a C IV doublet at $z_{abs} = 1.1672$ along with Al II $\lambda 1670$ at 3621 \AA , though we detect no other lines at these redshifts. The absorption features at 3937 \AA , 3942 \AA , 3946 \AA , and

3950 Å are traps in the CCD. The feature at 3722 Å is spurious as well, and it most likely a cosmic ray.

3.22. *Q 1323-107* $z_{em} = 2.360$

The only previously published spectrum found for this object is a spectrum including Ly α and C IV emission from Kunth et al. (1981). They find an emission redshift of 2.360 for the QSO. We find four candidate metal line systems from our absorption line spectrum:

$z_{abs} = 1.4244$ - This system is based upon the Si IV doublet at 3379 Å and 3401 Å. At this redshift, we also detect C II λ 1334 at 3235 Å and Si II λ 1526 at 3701 Å. No C IV doublet is detected.

$z_{abs} = 1.4727$ - This system is identified by the C IV doublet at 3828 Å and 3835 Å. Other lines detected include O I λ 1302 at 3220 Å and C II λ 1334 at 3300 Å.

$z_{abs} = 1.4922$ - This system is based upon the C IV doublet at 3858 Å and 3864 Å. Due to the large uncertainty in the position of the line center for the λ 1550 component, the redshifts of the doublet components agree to within $<1\sigma$. We also detect O I λ 1302 at 3246 Å, possible Si II λ 1304 and λ 1526 lines at 3250 Å and 3803 Å respectively, and Fe II λ 1608 at 4008 Å. Our red spectrum of this object (see Paper II) actually extends slightly blueward of 1.0 Å resolution blue spectrum and shows a possible Si II λ 1260 line at 3144 Å.

$z_{abs} = 1.8415$ - This system consists of Ly α at 3454 Å, N I λ 1135 and λ 1200 at 3225 Å and 3409 Å, a possible O I λ 1302 line at 3701 Å, Si II λ 1260 and λ 1304 at 3582 Å, and 3706 Å respectively, and C II λ 1334 at 3792 Å. The Si II λ 1260 line must be blended because its equivalent width is larger than that of Ly α . The N I and Si II line matches have been retained despite poor redshift agreement between the two lines of the same species due to the fact the errors in the line centers of lines 32 (N I λ 1200) and 64 (Si II λ 1260) are large enough for these redshifts to agree to within $\sim 3\sigma$. Our red spectrum shows no lines redward of Ly α for this system.

3.23. *Q 1329+412* $z_{em} = 1.934$

SBS88 (cf. Section 3.6) find six absorption line systems in their spectrum of this object. SS92 (cf. Section 3.2) confirm two of these systems and find another. These are the systems these authors report and the additional information gained from our spectrum:

$z_{abs} = 0.5009$ - SBS88 regard this system as probable from their identification of the Mg II doublet. The only search lines that fall in our spectral range for this redshift are Fe II λ 2344- λ 2600. We find none of these.

$z_{abs} = 1.2821$ - This system is identified by SS92 from a strong Mg II doublet. The spectrum of SBS88 did not cover the region of C IV absorption, but ours does and we find no significant lines that would correspond to the C IV doublet at this redshift.

$z_{abs} = 1.4716$ - This system is identified by SBS88 on the basis of an “unambiguous” C IV doublet. SS92 find no Mg II absorption at this redshift. We confirm the C IV doublet identification of SBS88 and also find a tentative O I λ 1302 line at 3217 Å.

$z_{abs} = 1.6010$ - SBS88 find a strong C IV doublet at this redshift which they note is likely to be blended with another C IV doublet at a nearby redshift. SS92 identify

the Mg II doublet at this redshift. Our spectrum shows the strong C IV doublet found by SBS88 in addition to Si II λ 1260 at 3279 Å, C II λ 1334 at 3471 Å, and the Si IV doublet at 3625 Å and 3648 Å. In addition, we find that the position of the C IV λ 1548 for $z_{abs} = 1.5980$ corresponds to a significant line in our spectrum while the λ 1550 component at this redshift appears to be strongly blended with C IV λ 1548 at $z_{abs} = 1.6007$.

$z_{abs} = 1.8359$ - This system is identified by SBS88 by the C IV doublet and confirmed by SS92 who find the Mg II doublet at $z_{abs} = 1.8355$. We detect Ly α at 3447 Å, a possible Fe II λ 1145 line at 3246 Å, possible Si II λ 1193 and λ 1260 lines at 3384 Å and 3575 Å, and C II λ 1334 at 3785 Å.

$z_{abs} = 1.8401$ - This system is identified by SBS88 on the basis of a C IV doublet. SS92 do not detect Mg II. We do detect a strong Ly α line consistent with this redshift at 3453 Å.

$z_{abs} = 1.9406$ - SBS88 identify this system on the basis of the C IV doublet. SS92 do not observe the spectral region encompassing Mg II at this redshift; but we detect Ly α at 3575 Å and a N V doublet at 3643 Å and 3654 Å. This system, having a redshift larger than the QSO emission redshift, is probably associated with the QSO.

The absorption features at 3969 Å, 3974 Å, 3979 Å, and 3983 Å are traps in the CCD.

We detect a possible C IV doublet redward of Ly α emission but blueward of the spectral range of SS92 at a redshift of 1.35285. The components are detected at 3643 Å and 3648 Å along with Fe II λ 1608 at 3785 Å. The λ 1548 component of the doublet coincides with N V λ 1238 at $z_{abs} = 1.9404$; and the λ 1550 component coincides with the Si II λ 1402 for the well-established system at $z_{abs} = 1.6010$ described above. No other lines are found. Also, we find another possible C IV doublet in the Ly α forest at $z_{abs} = 1.2480$; but no other lines are detected at this redshift either.

Lastly, Lanzetta, Wolfe, & Turnshek (1995) report a damped Lyman alpha system at $z_{abs} = 0.5193$ in the IUE spectrum of Lanzetta, Turnshek, & Sandoval (1993). Again, the only lines in our spectral range for this redshift are Fe II λ 2344- λ 2600. We detect only the strongest of these lines, Fe II λ 2382 at 3621 Å.

3.24. *Q 1337+285* $z_{em} = 2.541$

Our literature search yielded no previously published optical spectrum of this QSO. From our spectrum, we detect two possible heavy metal absorption systems:

$z_{abs} = 2.5081$ - This relatively secure system consists of Ly α at 4265 Å, Ly β at 3598 Å, possible O VI λ 1031 and λ 1037 lines at 3619 Å and 3640 Å, C II λ 1036 at 3636 Å, N II λ 1083 at 3803 Å, a possible Fe II λ 1145 line at 4017 Å, and Si II λ 1190 and λ 1193 at 4176 Å and 4186 Å.

$z_{abs} = 2.5228$ - For this system, we detect Ly α at 4283 Å, Ly β at 3614 Å, O VI λ 1031 at 3636 Å, possible N I λ 1135 and λ 1200 lines at 3998 Å and 4226 Å, Fe II λ 1143 and λ 1145 at 4027 Å and 4033 Å, and Si III λ 1206 at 4249 Å.

The absorption features at 4339 Å, 4344 Å, 4347 Å, and 4352 Å are traps in the CCD.

3.25. *Q 1346-036* $z_{em} = 2.362$

The spectrum of this QSO blueward of Ly α emission has been studied by YSB83 (cf. Section 3.8). We confirm

all the absorption features seen by these authors with the exception of the line they detect at 3844 Å which falls on a bad region in our spectrum. They find no metal line absorbers from their data, but suggest a possible Mg II doublet at $z_{abs} = 0.4453$. We detect this tentative doublet at 4043 Å and 4054 Å ($z_{abs} = 0.4458$) but find no Fe II absorption at this redshift. We detect the 4051 Å line reported by YSB83, but identify Mg II $\lambda 2803$ with the absorption feature at 4054 Å for better redshift agreement.

LTW87 (cf. Section 3.8) report no absorption features in their red (6250 Å - 8350 Å) spectrum of this object. And W86 (cf. Section 3.3) find no damped Lyman alpha candidates in their 3200 Å - 5200 Å spectrum.

The only additional identifications we make for this object are two Ly α -Ly β pairs at 3965 Å and 3345 Å ($z_{abs} = 2.2616$) and at 4028 Å and 3450 Å ($z_{abs} = 2.3630$). For the $z_{abs} = 2.2616$ pair, the Ly β line is stronger than Ly α and must be a blend; also, our red spectrum (see Paper II) shows the C IV doublet for this system at 5050 Å and 5058 Å. The $z_{abs} = 2.3630$ redshift is larger than the QSO emission redshift indicating that it must be associated with the QSO, although not an associated absorber per se, as it shows no metal lines. Our red spectrum does not show the C IV doublet at this redshift.

3.26. *Q 1358+115* $z_{em} = 2.589$

W86 (cf. Section 3.3) find several 4σ absorption features in their 10 Å resolution spectrum of this object. We confirm these lines with the exception of the features they report at 3573 Å, 3874 Å, and 4092 Å. We also confirm the feature they report at 4074 Å having less than 4σ significance.

We find six possible metal line systems from our data:

$z_{abs} = 0.5084$ - This system is a Mg II absorber for which the doublet is detected at 4218 Å and 4228 Å. The $\lambda 2803$ component of the doublet is blended with Ly α at $z_{abs} = 2.4778$. We also detect Fe II $\lambda 2382$ and $\lambda 2600$ at 3593 Å and 3922 Å and Mg I $\lambda 2853$ at 4303 Å.

$z_{abs} = 2.4158$ - This system is composed of a strong Ly α line at 4152 Å, possible Si II $\lambda 1190$ and $\lambda 1193$ lines at 4065 Å and 4075 Å, a N I possible $\lambda 1200$ line at 4098 Å, and Si III $\lambda 1206$ at 4121 Å. The expected position of N I $\lambda 1135$ for this redshift falls on a bad column in the data.

$z_{abs} = 2.5559$ - For this system, we find Ly α at 4323 Å, Ly β at 3647 Å, Si II $\lambda 1190$ and $\lambda 1193$ at 4234 Å and 4243 Å, N I $\lambda 1200$ at 4266 Å, and Si III $\lambda 1206$ at 4290 Å.

$z_{abs} = 2.5630$ - This system is composed of Ly α at 4331 Å, Ly β at 3655 Å and Si II $\lambda 1190$ and $\lambda 1193$ at 4241 Å and 4251 Å. The Si II $\lambda 1193$ line is blended with Ly α at $z_{abs} = 2.4968$.

$z_{abs} = 2.5763$ - At this redshift, we find an associated absorber showing Ly α at 4348 Å, Ly β blended with the feature at 3672 Å (Ly β at $z_{abs} = 2.5799$), O VI $\lambda 1031$ and $\lambda 1037$ at 3689 Å and 3709 Å.

$z_{abs} = 2.57996$ - This system is another associated absorber for which we identify Ly α at 4353 Å, Ly β at 3672 Å, and O VI $\lambda 1031$ and $\lambda 1037$ at 3694 Å and 3714 Å.

3.27. *Q 1406+492* $z_{em} = 2.161$

Literature searches yielded no previously published absorption spectrum of this QSO. From our data, we find two possible heavy element absorption systems:

$z_{abs} = 1.4330$ - This redshift is based upon the C IV doublet at 3767 Å and 3773 Å. We also detect the Si IV doublet at 3391 Å and 3411 Å. However, the Si IV $\lambda 1402$ line must be a blend (possibly with Si IV $\lambda 1393$ at $z_{abs} = 1.4474$) due to its equivalent width relative to the $\lambda 1393$ component and its poor redshift agreement with it.

$z_{abs} = 1.4470$ - This system is another C IV absorber for which the C IV doublet is found at 3788 Å and 3795 Å. We also find C II $\lambda 1334$ at 3266 Å, the Si IV doublet for which the $\lambda 1393$ component lies at 3411 Å and the $\lambda 1402$ component is blended with the feature at 3435 Å, Si II $\lambda 1526$ at 3736 Å, and Fe II $\lambda 1608$ at 3936 Å.

A C IV doublet is found at $z_{abs} = 1.5253$; and we find a Ly α , Ly β pair due to an absorber at $z_{abs} = 2.1540$. The absorption features present at 3962 Å, 3967 Å, 3968 Å, 3974 Å, 3978 Å, and 3981 Å are traps in the CCD.

3.28. *Q 1408+009* $z_{em} = 2.260$

According to a literature search, this is the first published spectrum of this object. Five possible metal line systems are found:

$z_{abs} = 1.3158$ - This system is identified by a Si IV doublet at 3228 Å and 3248 Å as well as Si II $\lambda 1526$ absorption at 3535 Å and a Fe II $\lambda 1608$ line at 3725 Å.

$z_{abs} = 1.5190$ - This system is a C IV absorber with $\lambda 1548$ identified at 3900 Å and $\lambda 1550$ at 3906 Å. Also found are C II $\lambda 1334$ at 3363 Å and Si II $\lambda 1526$ at 3843 Å.

$z_{abs} = 1.6929$ - This system consists of Ly α at 3274 Å, Si III $\lambda 1206$ at 3248 Å, Si II $\lambda 1260$ at 3394 Å, and O I $\lambda 1302$ at 3506 Å. Despite the fact that this Ly α line is relatively strong ($EW_0 = 1.153$ Å) all of the other lines identified are stronger, creating the need to invoke the possibility of blending for all of them. For this reason, this system is considered uncertain.

$z_{abs} = 1.9956$ - At this redshift, we detect Ly α at 3642 Å, N I $\lambda 1200$ at 3595 Å, Si II $\lambda 1260$ and $\lambda 1304$ at 3774 Å and 3906 Å, and O I $\lambda 1302$ at 3900 Å.

$z_{abs} = 2.1991$ - For this system, we identify Ly α at 3889 Å, a blended Ly β line at 3282 Å, Si III $\lambda 1206$ at 3859 Å, and Si II $\lambda 1260$ at 4032 Å.

The absorption features at 4575 Å, 4586 Å, 4602 Å are traps in the CCD.

3.29. *Q 1421+330* $z_{em} = 1.905$

The rest-UV absorption spectrum of this object has been studied by many authors. Weymann et al. (1979) find C IV in their 2.5 Å resolution spectrum at $z_{abs} = 1.462$, but not the expected Si IV and C II absorption. This redshift is confirmed by Koratkar et al. (1992) and by our data. We find Si IV at 3433 Å and 3455 Å and C IV at 3813 Å and 3820 Å.

Uomoto (1984) finds several tentative systems in his red spectrum of this QSO:

$z_{abs} = 0.2249$ - Uomoto (1984) detects a Mg II doublet at this redshift. Our spectrum shows this identification to be unlikely given the implied velocity separation of the doublet lines (~ 310 km s $^{-1}$) if they are associated with the features at 3428 Å and 3433 Å in our data.

$z_{abs} = 0.3236$ - Uomoto (1984) finds a Mg II doublet at this redshift. Our spectrum does not show these lines, nor any others at this redshift.

$z_{abs} = 0.9030$ - Uomoto (1984) finds several Fe II lines at this redshift, $\lambda 2344$, $\lambda 2374$, $\lambda 2382$, $\lambda 2586$, and $\lambda 2600$. Also, Mn II $\lambda 2594$ Å and a Mg II doublet are detected. This Mg II doublet is confirmed by SS92 (cf. Section 3.2.) Our spectrum shows Al III $\lambda 1854$ and $\lambda 1862$ absorption at 3530 Å and 3544 Å.

$z_{abs} = 1.1732$ - Uomoto (1984) finds a Mg II doublet at this redshift which is confirmed by SS92. We find Si II $\lambda 1526$ at 3318 Å; but no C IV or Al III.

$z_{abs} = 1.2252$ - Uomoto (1984) finds a C IV doublet at this redshift. We detect absorption at the position of the $\lambda 1548$ component, but none at the position of $\lambda 1550$.

Foltz et al. (1986) find four additional systems in their 1 Å resolution spectrum covering 3820 Å to 4035 Å:

$z_{abs} = 0.4565$ - A Mg II doublet is detected at this redshift. These lines should fall at the very red edge of our spectrum. While there are some possible features present, we are not able to confirm this system.

$z_{abs} = 1.5847$ - A C IV doublet is detected at this redshift. We detect O I $\lambda 1302$ at 3368 Å, C IV $\lambda 1548$ at 4001 Å, and an apparent absorption feature, but no significant line, at the position of C IV $\lambda 1550$.

$z_{abs} = 1.7177$ - Foltz et al. (1986) find a C IV doublet and Al II $\lambda 1670$ at this redshift. We confirm this system with our detections of Ly α at 3304 Å, Si III $\lambda 1206$ at 3279 Å, and O I $\lambda 1302$ at 3539 Å.

$z_{abs} = 1.7590$ - Foltz et al. (1986) detect a C IV doublet at this redshift. We detect a Ly α line consistent with this system at 3355 Å.

Caulet (1989) detects C IV at four redshifts including $z_{abs} = 1.7171$ and $z_{abs} = 1.4621$ (see above). The other systems detected are $z_{abs} = 1.7010$ and $z_{abs} = 1.7755$ for which we detect no Ly α absorption.

Lastly, Lanzetta et al. (1995) report a possible Lyman limit absorber in their IUE spectrum at $z_{LLS} = 1.4798$. We find possible absorption features at the positions of O I $\lambda 1302$, Si II $\lambda 1304$, and Si II $\lambda 1526$ for this redshift. These features are not identified as 3σ lines by FINDSL, however. We do not detect C IV, Si IV, or C II.

The absorption features at 3967 Å, 3972 Å, and 3980 Å are traps in the CCD.

3.30. *Q 1422+231* $z_{em} = 3.623$

This object is a gravitationally lensed quasar (Bechtold & Yee 1995, hereafter BY95.) Therefore, due to uncertainties in the amplification by the lensing, it will only be used for the analysis of the Ly α forest statistics and not in the proximity effect analysis in Paper II.

Bechtold & Yee (1995) obtained a spectrum of this object from 4818 Å to 5684 Å with 1.8 Å resolution using the Subarcsecond Imaging Spectrograph on the Canada-France-Hawaii Telescope. A red spectrum from 6246 Å to 7179 Å with 2.0 Å resolution was also obtained in order to identify metal line systems using the Red Channel Spectrograph on the Multiple Mirror Telescope. The systems identified by these authors are as follows:

$z_{abs} = 3.091$ - This system is identified by a strong C IV doublet. We detect a marginally consistent doublet at 6323 Å and 6331 Å in our red spectrum (see Paper II). BY95 also find Ly α , Si II $\lambda 1193$, N I $\lambda 1200$, Si II $\lambda 1260$, and O I $\lambda 1302$. We confirm the Ly α feature at 4973 Å and find features at 4882 Å, 4907 Å, 5157 Å, and 5328

Å, in marginal agreement with the other lines found by these authors. No Si II $\lambda 1190$ is detected by us or BY95. The O I $\lambda 1302$ line, if present, is blended with Ly α at $z_{abs} = 3.3830$.

$z_{abs} = 3.382$ - This system is also based upon a strong C IV doublet seen in the red spectrum of BY95. These authors also identify Ly α and Si II $\lambda 1260$ blended with a double-component Ly α line at 5519 Å. We confirm their C IV doublet from our red spectrum; and in our Ly α forest spectrum, we detect a strong Ly α line consistent with this redshift at 5328 Å, but do not confirm a Si II $\lambda 1260$ line corresponding to the one found by BY95.

$z_{abs} = 3.515$ - This system is based upon a weak C IV doublet for which BY95 also identify Ly α , Si II $\lambda 1190$ and $\lambda 1193$, and Si III $\lambda 1206$. We confirm the Ly α line at 5489 Å; we find N I $\lambda 1200$ at 5418 Å; but we do not find features corresponding to the Si II and Si III lines above. We do detect weak features at the correct position of C IV for this system in our red spectrum.

$z_{abs} = 3.536, 3.538$ - These systems are identified by strong C IV doublets by BY95. We confirm these in our red spectrum, but the two components are not resolved. These authors also identify Ly α and Si III $\lambda 1206$ for both components. We confirm these features, Ly α at 5513 Å and 5517 Å, and Si III at 5471 Å and 5475 Å; and we make an additional identification of N I $\lambda 1200$ at 5445 Å. Songaila & Cowie (1996) identify a strong redshift system at $z_{abs} = 3.5353$ in their high resolution (~ 0.15 Å) spectrum taken with HIRES on the Keck Telescope. They are able to derive column densities for several species, including C II, C IV, S II, Si III, Si IV, and N V (upper limit).

$z_{abs} = 3.587$ - BY95 find a weak C IV doublet at this redshift, and we confirm this detection in our red spectrum. They also identify Ly α and Si II $\lambda 1193$. We confirm these features at 5577 Å and 5475 Å and make the additional identifications of N II $\lambda 1083$ at 4973 (blended with Ly α at $z_{abs} = 3.0906$), Si III $\lambda 1206$ at 5534 Å and N I $\lambda 1200$ at 5504 Å. Songaila & Cowie (1996) find a strong system at $z_{abs} = 3.5862$ and derive column densities or upper limits for C II, C III, C IV, Si II, Si III, Si IV, and N V.

$z_{abs} = 3.624$ - BY95 find another weak C IV doublet at this redshift, along with Ly α , Si II $\lambda 1190$ and $\lambda 1193$, and Si III $\lambda 1206$. We detect the weak C IV absorption in our red spectrum. In our Ly α forest spectrum, we confirm Ly α at 5621 Å and the Si II lines at 5504 Å and 5578 Å; but we find no Si III line.

Songaila and Cowie identify a third strong redshift system from their data at $z_{abs} = 3.4464$ for which they derive column densities for C IV, Si III, and Si IV and upper limits on the column densities for C II, C III, and Si II. We detect a strong C IV doublet in our red spectrum; but in the Ly α forest, we identify only a strong Ly α line at 5407 Å corresponding to this system. These authors also identify a partial Lyman limit system at $z_{abs} = 3.3809$ showing C IV, Si IV, and C II. Our spectrum shows Ly α at 5324 Å and a possible Si II $\lambda 1260$ line at 5522 Å.

Lastly, we make two more metal line system identifications based upon strong Ly α absorption in our spectrum:

$z_{abs} = 3.3460$ - This system is composed of Ly α at 5283 Å, possible Si II $\lambda 1190$ and $\lambda 1193$ lines at 5174 Å and 5187 Å, Si III $\lambda 1206$ at 5244 Å, and Si II $\lambda 1260$ at 5477 Å.

$z_{abs} = 3.4945$ - At this redshift, we identify Ly α at 5464

\AA , Fe II $\lambda 1143$ and $\lambda 1145$ at 5137\AA and 5146\AA , possible Si II $\lambda 1190$ and $\lambda 1193$ lines at 5348\AA and 5363\AA , and N I $\lambda 1200$ at 5392\AA .

3.31. *Q 1435+638* $z_{em} = 2.066$

The absorption line spectrum of this QSO has been studied by several authors. SBS88 (cf. Section 3.6) report four C IV systems:

$z_{abs} = 1.4590$ - SBS88 find a weak, possible C IV doublet at this redshift. We confirm this identification, but note that these lines are more likely O I $\lambda 1302$ and Si II $\lambda 1304$ at $z_{abs} = 1.9233$. We find no other lines at this redshift.

$z_{abs} = 1.4792$ - SBS88 find a second weak, possible C IV doublet at this redshift. Our spectrum shows only the $\lambda 1548$ component at 3837\AA . There is a weak absorption feature at the position of the $\lambda 1550$ component, but no significant line is identified. No other lines are found at this redshift.

$z_{abs} = 1.5925$ - SBS88 find a probable C IV doublet at this redshift. We identify O I $\lambda 1302$ at 3376\AA and find a possible, weak absorption feature (but no 3σ line) at the position of C II $\lambda 1334$.

$z_{abs} = 1.9235$ - SBS88 regard this C IV doublet as certain. They also find C II $\lambda 1334$ and a possible Si IV $\lambda 1393$ line. We detect a strong Ly α line for this redshift at 3554\AA , Si II $\lambda 1260$ at 3685\AA , O I $\lambda 1302$ at 3808\AA , Si II $\lambda 1304$ at 3813\AA , C II $\lambda 1334$ at 3901\AA . In addition, SS92 find a strong Mg II doublet at this redshift.

Lanzetta et al. (1995) report no damped Lyman alpha candidates in their ultraviolet spectrum. The absorption features at 3824\AA and 3829\AA are traps in the CCD.

3.32. *Q 1604+290* $z_{em} = 1.962$

A literature search yielded no previously published absorption line spectrum of this QSO. Our spectrum shows no significant absorption lines. However, the signal-to-noise of the data blueward of Lyman alpha is poor (≤ 2 over the range 3200 - 3500\AA) and the spectrum is truncated blueward of 3493\AA . The apparent absorption features redward of Ly α emission are identified as traps in the CCD.

3.33. *Q 1715+535* $z_{em} = 1.932$

The Lyman alpha forest spectrum of this QSO has been studied by several authors. SBS88 (cf. Section 3.6) find three systems from their 3750 - 4930\AA spectrum:

$z_{abs} = 0.3673$ - SBS88 identify a Mg II doublet at this redshift. The $\lambda 2796$ component falls on a series of traps in the CCD at 3824\AA in our spectrum; and we do not detect the $\lambda 2803$ component. Mg I $\lambda 2853$ coincides with a feature at 3902\AA ; but we find no Fe II lines to corroborate this Mg II system, which is therefore still regarded as uncertain. Nelson & Malkan (1992) find no candidates for this system in their photometric search for [O II] emission from Mg II absorption systems. They do note a galaxy at a redshift of 0.449 , but we detect no Fe II at this redshift.

$z_{abs} = 1.6330$ - SBS88 detect a C IV doublet and Si II $\lambda 1526$ at this redshift. Our spectrum shows C II $\lambda 1334$ at 3512\AA , and a Si IV doublet at 3669\AA and 3692\AA . The IUE spectrum of Lanzetta et al. (1993) appears to show an absorption feature at $\sim 3200 \text{\AA}$, which would coincide with Ly α .

$z_{abs} = 1.7587$ - SBS88 report a C IV doublet at this redshift as well. We confirm this system with our detections of Ly α at 3354\AA and a possible Si II $\lambda 1260$ line at 3476\AA . We find possible weak absorption features at the positions of the Si IV doublet.

SBS88 also report a possible Galactic Ca II $\lambda 3935$ line. We confirm the detection of this line at 3934\AA . SS92 (cf. Section 3.2) detect no lines in their 5950 - 8040\AA and 5130 - 8950\AA spectra of this object.

In addition to the absorption line systems discussed above, we find four other systems from our spectrum:

$z_{abs} = 1.3412$ - At this redshift, we detect a C IV doublet at 3635\AA and 3631\AA and Al II $\lambda 1670$ at 3911\AA . We note the presence of a weak absorption feature (but no 3σ line) at the expected position of Si II $\lambda 1526$. Although we find only three lines for this system, the IUE spectrum of Lanzetta et al. (1993) appears to show a feature at $\sim 2850 \text{\AA}$ which could be identified with Ly α at this redshift.

$z_{abs} = 1.4711$ - This system consists of a possible C IV $\lambda 1548$ line at 3826\AA (no $\lambda 1550$ absorption is detected), Si II $\lambda 1526$ at 3772\AA , and C II $\lambda 1334$ at 3297\AA . We find weak features, but no significant lines at the positions of O I $\lambda 1302$ and Si II $\lambda 1304$. Only three line detections for this system are regarded as acceptable as well given a possible absorption line in the IUE spectrum of Lanzetta et al. (1993) at $\sim 3005 \text{\AA}$ which can be regarded as Ly α at this redshift.

$z_{abs} = 1.8746$ - For this system, we find Ly α at 3494\AA , possible Si II $\lambda 1193$ and $\lambda 1260$ lines at 3431\AA and 3625\AA , N I $\lambda 1200$ at 3449\AA , and possible Si III $\lambda 1206$ absorption at 3467\AA . SS92 find no Mg II $\lambda 2796$ at this redshift.

$z_{abs} = 1.8963$ - At this redshift, we detect Ly α at 3521\AA , N I $\lambda 1200$ at 3476\AA , a blended Si III $\lambda 1206$ line at 3494\AA , and O I $\lambda 1302$ at 3772\AA .

The apparent absorption features at 3818\AA , 3821\AA , 3824\AA , and 3826\AA are identified as traps in the CCD.

3.34. *Q 2134+004* $z_{em} = 1.941$

We find no previously published spectrum for this object. Our data show 19 absorption lines. Line #17 is tentatively identified at Mg II $\lambda 2796$ at $z_{abs} = 0.3654$. The $\lambda 2803$ component of the doublet as well as Mg I $\lambda 2853$ coincide with absorption features which are not identified as 3σ lines by FINDSL. No Fe II lines are found at this redshift.

3.35. *Q 2251+244* $z_{em} = 2.359$

Carswell et al. (1976) report one metal line system in their spectrum (3250 - 5200\AA) of this object. This system is an associated absorber at $z_{abs} = 2.3638$; and these authors identify Ly α , Ly β , C III $\lambda 977$, O VI $\lambda 1031$, N I $\lambda 1200$, N V $\lambda 1238$, Si IV $\lambda 1393$, and C IV $\lambda 1548$. This system is confirmed by Barthel et al. (1990) from their 5.0\AA resolution spectrum over the range 3870 - 7730\AA who detect Ly α , N V $\lambda 1238$, Si IV $\lambda 1393$, and C IV $\lambda 1548$ as well. The N V, Si IV, and C IV doublets are also confirmed by Aldcroft et al. (1994). We confirm this system as well with our identifications of Ly α at 4088\AA , Ly β at 3450\AA and O VI $\lambda 1031$ and a blended $\lambda 1037$ line at 3470\AA and 3490\AA respectively. In addition, our red spectrum of this object (see Paper II) shows the N V doublet at 4167

Å and 4181 Å, the Si IV doublet at 4688 Å and 4718 Å, and the C IV doublet at 5205 Å and 5214 Å. The region of the spectrum blueward of ~ 3290 Å has been removed from our analysis due to low signal-to-noise ($\lesssim 2$).

Barthel et al. (1990) report four other systems:

$z_{abs} = 1.7495$ - At this redshift, the authors detect a C IV doublet. We detect only a possible N V $\lambda 1242$ line at 3416 Å. Since no lines are detected at shorter wavelengths in our spectrum, no $\lambda 1238$ component is identified. Aldcroft et al. (1994) confirm this system. Our red spectrum does show a possible C IV doublet associated with this system at 4257 Å and 4264 Å.

$z_{abs} = 1.0901$ - For this system, the authors identify Fe II $\lambda 2382$, a Mg II doublet and Mg I $\lambda 2852$. Our spectrum shows only a possible Al II $\lambda 1670$ line at 3490 Å. The only other lines that fall within the range of our line list are Al III $\lambda 1854$ and $\lambda 1862$, but these are not found. Aldcroft et al. (1994) confirm this system. Our red spectrum confirms the Mg II doublet identification made by Barthel et al. (1990) (5842 Å and 5857 Å) but not the Fe II or the Mg I identifications.

$z_{abs} = 2.1554$ - The authors find C II $\lambda 1334$ and a C IV doublet at this redshift. Aldcroft et al. (1994) confirm this and also detect Si IV $\lambda 1393$. In our spectrum, we identify Ly α for this system at 3835 Å, Si II $\lambda 1193$ at 3765 Å (the position of $\lambda 1190$ falls on a bad column in the data), N I $\lambda 1200$ at 3786 Å, a possible Si III $\lambda 1206$ line at 3807 Å, and Si II $\lambda 1260$ at 3976 Å. In addition, our red spectrum shows C II $\lambda 1334$ at 4122 Å, Si II $\lambda 1526$ at 4816 Å, the C IV doublet at 4885 Å and 4893 Å, Al II $\lambda 1670$ at 5272 Å, and a possible Al III $\lambda 1854$ line at 5272 Å. (No Al III $\lambda 1862$ line is found.)

$z_{abs} = 2.3524$ - Barthel et al. (1990) identify C IV and N V doublets at this redshift which are confirmed by Aldcroft et al. (1994). In our spectrum, we identify Ly α at 4074 Å, Ly β at 3438 Å, O VI $\lambda 1031$ and $\lambda 1037$ at 3459 Å and 3478 Å, and a possible Fe II $\lambda 1145$ line at 3838 Å. We also confirm the N V and C IV doublet found by Barthel et al. (1990) from our red spectrum, though the N V doublet we identify has a doublet ratio less than one. In addition, our red spectrum shows O I $\lambda 1302$ at 4367 Å and C II $\lambda 1334$ at 4475 Å.

We also identify a number of other systems from our data:

$z_{abs} = 1.8993$ - This system is composed of Ly α at 3525 Å, possible Si II $\lambda 1190$ and $\lambda 1193$ absorption at 3450 Å and 3459 Å, N I $\lambda 1200$ at 3478 Å, O I $\lambda 1302$ at 3775 Å, and Si II $\lambda 1260$ 3653 Å. In addition, our red spectrum shows Si II $\lambda 1526$ at 4427 Å.

$z_{abs} = 2.0336$ - At this redshift, we identify Ly α at 3688 Å, possible, blended Si II $\lambda 1193$ and $\lambda 1260$ lines at 3620 Å and 3824 Å, Si III $\lambda 1206$ at 3660 Å, and O I $\lambda 1302$ at 3949 Å. Our red spectrum shows Si II $\lambda 1526$ at 4631 Å, a possible, blended Fe II $\lambda 1608$ line at 4879 Å, and Al II $\lambda 1670$ at 5068 Å.

$z_{abs} = 2.0570$ - For this system, we find Ly α at 3716 Å, N I $\lambda 1135$ (blended) and $\lambda 1200$ at 3470 Å and 3668 Å, a blended Si III $\lambda 1206$ line at 3688 Å, and the N V doublet at 3786 Å and 3799 Å. Also, our red spectrum shows the Si IV doublet at 4262 Å and 4289 Å as well as Fe II $\lambda 1608$ at 4915 Å.

$z_{abs} = 2.1052$ - This system consists of Ly α at 3775 Å, Si

III $\lambda 1206$ at 3746 Å, and Si II $\lambda 1260$ and $\lambda 1304$ at 3913 Å and 4050 Å. Our red spectrum shows a possible, blended Al II $\lambda 1670$ line at 5188 Å.

$z_{abs} = 2.3158$ - This system is composed of Ly α at 4031 Å, a possible O VI $\lambda 1037$ line at 3440 Å ($\lambda 1031$ is outside the range of the line list), N I $\lambda 1200$ at 3979 Å, and Si III $\lambda 1206$ at 4001 Å. Our red spectrum extends slightly blueward of the higher resolution Ly α forest spectrum and shows some evidence for Ly β at 3401 Å and O VI $\lambda 1031$ at 3422 Å, as well as Si II $\lambda 1260$, $\lambda 1304$, and $\lambda 1526$ at 4181 Å, 4327 Å, and 5065 Å, O I $\lambda 1302$ at 4319 Å, and C II $\lambda 1334$ at 4427 Å.

3.36. *Q 2254+024* $z_{em} = 2.090$

The radio properties and the UV emission lines of this object have been widely studied. SS92 (cf. Section 3.2) find no absorption lines in their red spectra (5128-8947 Å). Due to the poor signal-to-noise (≤ 2) of the blue region of our spectrum, only the portion redward of 3450 Å was used for our line list. We find 25 absorption lines but no metal line systems according to our criteria. Only two possible identifications are made: a C IV doublet at $z_{abs} = 1.4751$ for which the $\lambda 1550$ component must actually be blended with the feature at 3837 Å; and a Si IV doublet at $z_{abs} = 1.7323$ for which the corresponding Ly α line falls in the low signal-to-noise region of the data and is not seen. However, our red spectrum (see Paper II) does lend some confirmation to the possible $z_{abs} = 1.7323$ system as it shows this Si IV doublet as well as Si II $\lambda 1526$ at 4171 Å, a C IV doublet at 4233 Å and 4238 Å, and Al II $\lambda 1670$ at 4564 Å. No lines redward of Ly α are confirmed for the $z_{abs} = 1.4751$ system.

3.37. *Q 2310+385* $z_{em} = 2.181$

No previously published spectrum of this QSO was found. Due to poor signal-to-noise blueward of 3571 Å, only the portion of the spectrum redward of this wavelength was used for the purposes of our line list. Fifteen significant absorption lines were found, but none of these could be identified with any heavy element absorption systems. Three identifications of doublets redward of Ly α emission could be made: C IV doublets at $z_{abs} = 1.4998$ and $z_{abs} = 1.5036$; and a Mg II doublet at $z_{abs} = 0.3840$.

3.38. *Q 2320+079* $z_{em} = 2.088$

We found no previously published spectrum of this object. We find a double component damped Ly α complex in our spectrum at 3712 Å and 3715 Å. Each of these components shows Si II $\lambda 1193$ (3645 Å) and Si III $\lambda 1206$ (3685 Å and 3687 Å.) Si II $\lambda 1190$ is present, but not identified as a 3σ line by FINDSL. The feature at 3553 Å is most likely a cosmic ray.

3.39. *Q 2329-020* $z_{em} = 1.896$

No previously published spectra of this QSO were found. We find 17 significant absorption lines in our spectrum. We make a number of identifications of doublets redward of Ly α emission. Two C IV doublets are seen at $z_{abs} = 1.2902$ and $z_{abs} = 1.2922$, a separation of ~ 260 km s $^{-1}$. The second doublet also appears to have weak features of Si II $\lambda 1526$ and Al II $\lambda 1670$ associated with it. A strong C IV doublet is also detected at $z_{abs} = 1.3339$ along

with weak features at the positions of Si II $\lambda 1526$ and Al II $\lambda 1670$. This QSO also shows associated Ly α absorption at 3509 Å, 3513 Å, 3521 Å, and 3531 Å, but no metals lines are found at this redshifts.

3.40. Data from the Literature

Spectra that met three basic criteria were gathered from the literature. In all cases, the errors were published, the resolution was equal to or better than 200 km s⁻¹, and no broad absorption line features were present, which would indicate the presence of material intrinsic to the QSO (see Table 5 of B94). Table 2 is a list of the objects chosen to supplement the sample and the reference for each. Figure 2 shows histograms of the distribution of QSO redshifts and absorption line redshifts for the total sample.

The line list for the QSO 1603+383 was provided by Dobrzycki, Engels, & Hagen (1999) prior to publication. This object has a B magnitude of 15.9.

4. RESULTS AND DISCUSSION

The number of Ly α lines per unit redshift per unit equivalent width can be parametrized as follows:

$$\frac{\partial^2 \mathcal{N}}{\partial z \partial W} = \frac{\mathcal{A}_0}{W^*} (1+z)^\gamma \exp\left(-\frac{W}{W^*}\right). \quad (1)$$

Integrating this equation over equivalent width with a constant threshold equivalent width throughout each spectrum gives

$$\frac{d\mathcal{N}}{dz} = \mathcal{A}_0 (1+z)^\gamma. \quad (2)$$

To solve for the parameters γ and W^* , we use a maximum likelihood technique which allows for an equivalent width threshold that varies with wavelength. We also derive these parameters using various fixed threshold values; and in this case, the procedure reduces to the method described in the Appendix of MHPB, using corrected expressions for their equations (A8) and (A2a). However, the variable threshold information is still used in the fixed threshold case, as regions of the spectrum for which the threshold lies above the fixed value, ie. where not all significant lines could be detected even if they were present, are excluded.

The solutions for the statistics γ and W^* are listed in Table 3. Each sample excludes regions of the spectra within Δz of 0.15 of the QSO emission redshift, chosen to eliminate any effects on the line density due to proximity to the QSO. A variable equivalent width threshold gives a value of 1.23 ± 0.16 for γ . This is lower than the value of 2.75 ± 0.29 found by LWT for a fixed equivalent width threshold of 0.36 Å over the range $1.7 < z < 3.8$, and the value of 1.89 ± 0.28 found by B94 for a fixed threshold of 0.32 Å over the range $1.6 < z < 4.1$. Using a fixed threshold of 0.32 Å, the value of γ derived from our data is 1.88 ± 0.22 , in good agreement with that of B94. In Table 3, no error is quoted for \mathcal{A}_0 because it is strongly correlated with the error in γ .

We calculate the Kolmogorov-Smirnov (KS) probability that a power law number density distribution given by Equ. 2 for each of these values of γ is a good representation of the data (cf. Appendix of MHPB). A high probability (P_{KS}) that the maximum deviation from the cumulative

number distribution could occur by chance if the data set is drawn from an assumed parent distribution indicates that the choice of parent distribution is justified. These results are included in Table 3. The total sample and each of the subsamples is described well by a single power law, as illustrated by the high KS probabilities obtained. The KS probability obtained from our data set with a fixed equivalent width threshold of 0.32 Å and the LWT γ value of 2.75 is 0.0020, while the B94 value of 1.85 gives 0.97, as it is in good agreement with our maximum likelihood result.

The errors in γ and W^* are calculated by our software by fitting a parabola to the peak of the logarithm of the likelihood function, using the fact that the likelihood function itself should be distributed as a Gaussian in γ and W^* near its maximum value. In order to avoid any assumptions about the distribution of the statistics of interest, a resampling technique was used to independently estimate the distribution. Jackknife samples (Babu & Feigelson 1996, Efron 1982) of our original data set were constructed, 100 in all, each with one QSO from the original sample removed. We used the same program to calculate γ and W^* for each jackknife sample, for the case of $W_{thr}=0.32$ Å. The goal is to understand how the values of these statistics found by our software vary with random variations in the data. The weighted mean of all the jackknife values for γ is 1.91 and for W^* it is 0.309 Å. Since we cannot treat each of the 100 values of these statistics as independent measurements of γ and W^* , the jackknife errors show how well the error calculated by the software estimates the true distribution of the statistics calculated. The jackknife results for σ_γ and σ_{W^*} are 0.26 and 0.011 respectively. The fact that the jackknife errors are $\sim 20\%$ larger than the error calculated by our software may reflect the fact that the jackknife estimate of the variance tends to be conservative (Efron 1982) or it may indicate the presence of additional sources of random error. In any case, the jackknife results do agree with the total data set result to well within the errors.

The two questions we now ask are whether the number densities of strong and weak lines evolve differently with redshift and whether there is a difference in γ for low and high redshift subsamples, ie. does γ evolve over the history of the universe after the observed break at $z \sim 1.7$? In this context, strong lines will refer to lines with rest equivalent widths greater than 0.32 Å and weak lines will refer to those with rest equivalent widths between 0.16 Å and 0.32 Å. The total absorption line sample was divided into low and high redshift subsamples at an absorption redshift of 2.5, giving 1084 and 995 lines in each subset, respectively. For the remainder of this paper, the low and high redshift subsamples will refer to Lyman α forest absorption lines with redshifts above and below 2.5, respectively.

Figure 3 is a set of plots of $\log(d\mathcal{N}/dz)$ versus $\log(1+z)$ for the various subsamples of our data set which are binned solely for display purposes. The straight lines are derived from the parameters given in Table 3. Figure 4a shows the low and high redshift subsamples and the solutions for each along with the solution for the total sample. Each of these are generated with a fixed equivalent width threshold of 0.32 Å. Figure 4b shows the results for strong ($W > 0.32$ Å) and weak lines ($0.16 < W < 0.32$ Å) considered

separately. Column 8 of Table 3 lists the KS probabilities for each case considered.

No $\log(dN/dz)$ versus $\log(1+z)$ plots are shown and no KS probabilities are quoted for any case in which a variable threshold was used. This is because the distribution in redshift is now related to the equivalent width of each line. The separation of these two distributions, which is possible in the case of a constant threshold, is not possible; and the formalism of MHPB can no longer be applied. Nevertheless, since the implementation of a variable threshold allows the most efficient use of the data, we consider these values of γ to be reliable, especially in light of the reasonable KS probabilities in the constant threshold cases.

Considering the moderate resolution and signal-to-noise of our data, it is worth investigating how well we are recovering the true parameters describing the line distribution. Recall from the discussion of the simulations in Section 2 that our 5σ line lists are 55% complete due to blending. To address this point, we generated more sets of artificial spectra based on the 56 objects in our data set for which we have detailed spectral information in the way described in Section 2.2. The redshift of each QSO in these sets is equal to that of one of the 39 new MMT spectra presented in this paper or to that of one of the 17 spectra presented in Dobrzycki and Bechtold (1996). In order to investigate how signal-to-noise impacts this analysis, we created three sets of these 56 artificial spectra with the resolution of the data, $\sim 1 \text{ \AA}$, one set having signal-to-noise ratios half that of the data (median S/N ~ 5), another having signal-to-noise ratios equal to that of the data (median S/N ~ 10), and another having twice the signal-to-noise of the data (median S/N ~ 20). The input parameters used were $\gamma=1.88$, $\beta=1.46$, $N_{lower}=1 \times 10^{13} \text{ cm}^{-2}$, $N_{upper}=1 \times 10^{16} \text{ cm}^{-2}$, $\langle b \rangle = 28 \text{ km s}^{-1}$, and $\sigma_b = 10 \text{ km s}^{-1}$.

In the low S/N simulation, FINDSL spuriously identified one simulated line, out of 1722 lines above threshold, as two separate lines, both of 5σ significance or greater. This did not occur in either the data S/N simulation, or in the high S/N simulation, so we remain confident that the Lyman α lines in our line lists are real absorption features.

We also generated set of synthetic spectra with higher resolution than the data. Two sets were made with resolution $\Delta\lambda \sim 0.7 \text{ \AA}$, one with the same signal-to-noise as the data, and another with median S/N ~ 20 . Finally, a Keck/HIRES data set was simulated by generating spectra with $\Delta\lambda \sim 0.2 \text{ \AA}$ and median S/N ~ 40 .

The simulation line lists were analyzed in the same way as the data to determine the value of γ input into the FINDSL analysis. This γ is not necessarily equal to the simulation input γ , 1.88, because, in generating the artificial spectra, the simulation software does not fix the redshift and equivalent width distributions by the input parameters, but rather draws line redshifts and equivalent widths from a distribution given by Equation 2. FINDSL line lists were then generated and γ was calculated again using these line lists. This was done for both the variable threshold and the case of an equivalent width threshold of 0.32 \AA for all redshifts, and at high and low redshifts separately. The two values of γ for each case are compared with each other in order to determine how well the redshift

distribution in the FINDSL line lists reflects the distribution output by the simulations. The results are listed in Table 4. The simulation resolution and median signal-to-noise ratio are given in the first two columns; the redshift range and the threshold used for the γ solution are given in columns (3) and (4); and the values of γ derived from the simulation line lists ($\gamma_{simulation}$) and from the FINDSL line lists (γ_{FINDSL}) are given in columns (5) and (6), respectively. DB96 discuss this simulation software in detail and use it to investigate the column density distribution of Lyman α lines. Their data set, a subset of ours, encompassed a limited redshift path and was therefore insensitive to a determination of γ from the simulations. Presumably, if we ran the large number of simulations for which this software was designed, we would recover $\gamma=1.88$ in column (5) of Table 4; but since we are merely trying to determine the reliability of our methods for identifying significant lines, we will leave this for future work. These Monte-Carlo simulations create line lists by distributing lines according to the input value of γ , which is independent of redshift and equivalent width. It is for this reason, and because we have created a relatively small number of synthetic spectra in order to simulate our data set, that we do not take the values of γ derived either from the simulation line lists or from the FINDSL line lists to truly reflect the redshift distribution of Lyman α lines. We use these simulations only to investigate how well our techniques for identifying significant lines and calculating γ recovers the value input into the FINDSL analysis.

Figure 4 also demonstrates these results. It shows the number of sigma difference between the output (FINDSL line lists) and input (simulation line lists) values of γ , (a)-(c) for the variable threshold case and (d)-(f) for the $W_{thr}=0.32 \text{ \AA}$ case. The square points and solid lines indicate the results for the simulations at the resolution of the data in this paper, $\Delta\lambda \sim 1 \text{ \AA}$. The open triangles and dotted lines show the results for the simulations at higher resolution, $\Delta\lambda \sim 0.7 \text{ \AA}$; and the filled triangle shows the result for the Keck/HIRES simulation, $\Delta\lambda \sim 0.2 \text{ \AA}$.

Histograms of the line distributions used in the input (simulation line lists) and output (FINDSL line lists) γ solutions are shown in Figure 5(a-d). Also, plots of $\log(dN/dz)$ versus $\log(1+z)$ analogous to those in Figure 3 for the data resolution, data S/N, constant threshold simulations are shown in Figure 6. As in Figures 5(a-d), the solid lines correspond to the maximum likelihood solution for γ and \mathcal{A}_0 for the simulation line lists and the dashed lines correspond to the solution for the FINDSL line lists. These figures demonstrate that the process of simulation lines above threshold being “blended out” with other features in the final FINDSL line lists dominates over lines below threshold being “blended in” by blending with other features below threshold in all cases. Overall, therefore, the FINDSL line lists suffer from a net loss of lines due to the blending out of significant features.

However, this blending has not significantly affected the value of γ . The only case for which the simulation and subsequent FINDSL solutions for γ differ by more than 1.5σ , indicated by the dashed-dotted lines in Figure 4, is the constant threshold solution for the lowest S/N simulation at low redshift, the leftmost point in Figure 4(b). It should be noted that some visual inspection of the simulation spectra

was necessary to achieve this overall agreement between the simulation and the FINDSL γ 's. This examination was commensurate with that done on the data, especially during the course of the metal line identifications, so no significant bias is introduced into the simulation analysis by doing this. The FINDSL program tended to miss some weak lines in the high redshift spectra due to crowding of features. Some lines were also missed by FINDSL at low redshift, where the signal-to-noise is lowest. The equivalent width thresholds used in the solution for γ required that the weakest lines at low S/N be left out of the simulation line list solution, so missing them with FINDSL had little effect. However, in some cases, FINDSL either failed to find lines above threshold at low S/N or failed to fit them with the proper equivalent width. These omissions did adversely affect the agreement between the γ solutions, as these lines were included in the solution using simulation line lists. Upon inspection of the simulated spectra, all of these lines were identified and the simulation and FINDSL line list solutions for γ were brought into agreement.

For the total sample and the high redshift subsample, including weak lines in the maximum likelihood solution tends to make γ more shallow. Both our data and high resolution work (Cristiani et al. 1995, Giallongo et al. 1996) indicate that the tendency for γ to change in either direction when weaker lines are included is not a significant one. Decreasing the column density cutoff from $\log(N_{HI})=13.8$ to 13.3 at $z\sim 3$, Cristiani et al. (1995) find that γ increases from 1.86 to 2.17; but this is a change of less than 1σ . Giallongo et al. (1996) find that decreasing the column density cutoff from $\log(N_{HI})=14$ to 13.3, again at $z\sim 3$, decreases γ from 2.7 to 2.49, $\sim 1\sigma$. However, using only weak lines for our total sample gives a γ of 0.26 ± 0.33 , a value consistent with no evolution for $q_0 = 0.5$; while using all lines with rest equivalent width greater than 0.32 \AA gives a value 4σ larger, 1.88. In the case of the high redshift subsample, this difference is 2.6σ . Weak lines being blended out in the crowded, high redshift regions of the spectra is undoubtedly contributing to this effect. In our simulations, lines with rest equivalent widths between 0.16 \AA and 0.32 \AA yield a γ of 2.25 ± 0.40 for the simulation output lines, while the FINDSL line lists give a significantly lower value of 1.30 ± 0.49 . The plots of $\log(dN/dz)$ versus $\log(1+z)$ analogous to Figure 6 for these weak lines are shown in Figure 7; and this solution for all redshifts is shown in panel (a). Recall that the input simulation redshift distribution is independent of the line width. By contrast, the simulation line list and FINDSL line list values of γ for lines with equivalent widths greater than 0.32 \AA are 1.62 ± 0.27 and 1.70 ± 0.30 , respectively. This indicates that though we can be confident that we are recovering the true γ for lines with equivalent widths greater than 0.32 \AA , weak lines blended out at high redshift in our data may indeed produce this flattening of γ seen when weak lines are included in the solution.

For the low redshift subsample, the weak lines give a steeper γ , but this difference is not statistically significant. The Weymann et al. (1998) results at $z < 1.7$ suggest the opposite, that lines of higher rest equivalent width yield larger values of γ . These authors find a difference in the evolution rates for Ly α absorbers with and without identified associated metal lines. Their interpretation of

this is that it can be attributed to a difference in the rate of evolution of lines of different strengths. This scenario is supported by the higher redshift results of Kim et al. (1997). Their high resolution data suggest that there is a break in the column density distribution of Ly α lines at $\log(N_{HI}) \geq 14.8$ and $z \sim 3.3$ and that this break occurs at lower column densities and becomes more pronounced as redshift decreases. These results imply that weak lines should show a flatter γ at all redshifts and that the difference in the rate of evolution between strong and weak lines should be more significant at redshifts less than 2.5 than at redshifts greater than 2.5.

The γ 's derived from the simulation and FINDSL line lists for the spectra generated at the data resolution and signal-to-noise listed in Table 4 are generally in good agreement with one another for strong and weak lines at low and high redshift, noting however, the large uncertainties for the weak line γ 's. The FINDSL γ 's for weak lines for all redshifts and at low redshift are systematically lower than the simulation γ 's, due to blending out of weak features preferentially at high redshift. The high redshift solution does not suffer from this as lines are evenly blended out at all redshifts greater than 2.5, as demonstrated in Figure 7(a-c). In any case, this comparison indicates that there is no tendency for blending to work to artificially produce the trend noted above, namely that the γ for weak lines is steeper than the γ for strong lines at low redshift, contrary to the results of other authors.

For a variable threshold at high redshifts, γ flattens by 1.5σ compared to the value found for low redshift lines, to 0.64 ± 0.47 for $z > 2.5$ from 1.57 ± 0.42 at $z < 2.5$. Again, the difference is not statistically significant; but a trend exists in that the maximum likelihood values of γ found for the low redshift subsample are larger than those found for the high redshift subsample in all cases in which weak lines are included, while for strong lines, γ increases from low to high redshift. The agreement between the γ 's derived from the simulation line lists and the FINDSL line lists indicates that, at the resolution and signal-to-noise of the data, this trend is not artificially imposed by blending.

Equivalently, one can investigate the distribution in equivalent width as a function of redshift. The value of the parameter W^* increases from low to high redshift from 0.282 \AA to 0.330 \AA in the case of a constant 0.32 \AA threshold, a difference of $\sim 3\sigma$ in the sense that the distribution is more shallow at high redshift. Both of these results imply that there exist more weak lines relative to strong ones at low redshift than at high redshift. Given the discussion above, it is likely that at least some of this difference can be attributed to increased blending of weak lines at high redshifts. Nevertheless, the Kim et al. (1997) analysis supports this interpretation, as do the results of the hydrodynamic simulations of Davé et al. 1999. These authors find that W^* does indeed increase with redshift from $z=0$ to $z=3$ due to the onset of structure formation. The values of W^* they derive from their simulated spectra at high resolution are smaller than those measured in this paper or at low redshift by Weymann et al. (1998). They find, however, that the effects of blending in even low redshift, moderate resolution spectra, comparable to the FOS data, can raise the measured values to those found by Weymann et al. (1998).

This effect is demonstrated by Figure 8, a histogram of

the rest equivalent width distribution of lines in the simulation and FINDSL line lists for the data resolution ($\sim 1 \text{ \AA}$) simulations with median signal-to-noise ratios of 5, 10, and 20 in the variable threshold case. As expected, the number of lines blended out is largest at low equivalent width, flattening out the overall distribution and in turn raising the value of W^* derived.

If a fixed equivalent width threshold of 0.32 \AA is used (rows 9, 11, 15, and 17 in Table 3), weak lines are thrown out and the distribution in redshift is flatter at low redshift than at high redshift, though not significantly so: $\gamma = 1.30 \pm 0.60$ for $z < 2.5$, versus 1.69 ± 0.60 for $z > 2.5$, a difference of less than 0.5σ . Interestingly, Stengler-Larrea et al. (1995) find $\gamma = 1.50 \pm 0.39$ for Lyman limit absorbers between $z=0.32$ and $z=4.11$, in reasonable agreement with our values of γ using $W_{thr}=0.32 \text{ \AA}$ for both the low and high redshift subsamples. The total sample of lines with $W > 0.32 \text{ \AA}$ gives a somewhat larger value of γ , 1.88 ± 0.22 , but including the low redshift data of Bahcall et al. (1993) yields a value of 1.70 ± 0.19 , consistent with the result for Lyman limit systems. It has been proposed that Ly α absorbers with $\log(N_{HI}) \gtrsim 14$, the value of the break in the column density distribution, are associated with the outer halos of galaxies responsible for Lyman limit systems and damped Lyman α systems (Giallongo et al. 1996, Lanzetta et al. 1995, 1996, Chen et al. 1998). This column density is approximately equivalent to the equivalent width threshold of 0.32 \AA used in this study; and the agreement between our values of γ and that for Lyman limit systems lends some credence to this scenario.

We extend thanks to the staff of the Multiple Mirror Telescope Observatory for their assistance with the observations, to T. Aldcroft for use of his program FINDSL, and to K. -V. Tran for assistance with data reduction and continuum fits. We also thank S. Morris for a helpful referee report. J. S. acknowledges the support of the National Science Foundation Graduate Research Fellowship and the Zonta Foundation Amelia Earhart Fellowship. J. B. acknowledges support from AST-9058510 and AST-9617060 of the National Science Foundation. A. D. acknowledges support from NASA Contract No. NAS8-39073 (ASC). This research has made use of the NASA/IPAC Extragalactic Database (NED) which is operated by the Jet Propulsion Laboratory, California Institute of Technology, under contract with the National Aeronautics and Space Administration.

REFERENCES

- Afanasjev, V. L., Karachentsev, I. D., Lipovetsky, V. A., Lorentz, H., & Stoll, D. 1979, *Astron. Nachr.*, 300, 31
- Aldcroft, T. L., Bechtold, J., & Elvis, M. 1994, *ApJS*, 93, 1
- Babu, G. J. & Feigelson, E. D. 1996, *Astrostatistics*, (London: Chapman & Hall)
- Bahcall, J. N., Bergeron, J., Boksenberg, A., Hartig, G. F., Jannuzi, B. T., Kirhakos, S., Sargent, W. L. W., Savage, B. D., Schneider, D. P., Turnshek, D. A., Weymann, R. J., & Wolfe, A. M. 1993, *ApJS*, 87, 1
- _____ 1996, *ApJ*, 457, 19
- Baker, A. C., Carswell, R. F., Bailey, J. A., Espey, B. R., Smith, M. G., & Ward, M. J. 1994, *MNRAS*, 270, 575
- Barthel, P. D., Tytler, D. R., & Thomson, B. 1990, *A&A*, 82, 339
- Beaver, E.A., Burbidge, E. M., Cohen, R. D., Junkkarinen, V. T., Lyons, R. W., Rosenblatt, E. I., Hartig, G. F., Margon, B., & Davidsen A. F. 1991, *ApJ*, 377, L1 (B91)
- Bechtold, J. 1994, *ApJS*, 91, 1 (B94)
- Bechtold, J. & Yee, H. K. 1995, *AJ*, 110, 1984
- Bi, H. G. 1993, *ApJ*, 405, 479
- Bi, H. G. & Davidsen, A. 1997, *ApJ*, 479, 523
- Carswell, R. F., Coleman, G., Strittmatter, P. A., & Williams, R. E. 1976, *ã*, 53, 275
- Calet, A. 1989, *ApJ*, 340, 90
- Chen, H.- W., Lanzetta, K. M., Webb, J. K., & Barcons, X. 1998, *ApJ*, 498, 77
- Cristiani, S., D'Odorico, S., Fontana, A., Giallongo, E., & Savaglio, S. 1995, *MNRAS*, 273, 1016
- Croft, R. A. C., Weinberg, D. H., Katz, N., & Hernquist, L. 1998, *ApJ*, 495, 44
- Croft, R. A. C., Weinberg, D. H., Pettini, M., Hernquist, L., & Katz, N. 1999, *ApJ*, 520, 1
- Davé, R., Hernquist, L., Katz, N., & Weinberg, M. 1999, *ApJ*, 511, 521
- Dobrzycki, A. & Bechtold, J. 1996, *ApJ*, 457, 102
- Dobrzycki, A. & Bechtold, J. 1997, in *Structure and Evolution of the Intergalactic Medium from QSO Absorption Line Systems*, Proc. of the 13th IAP Astrophysics Colloquium, ed. P. Petitjean & S. Charlot (Paris: Editions Frontieres), 390
- Dobrzycki, A., Engels, D., & Hagen, H.-J. 1999, *ã*, 349, L29
- Efron, B. 1982, *The Jackknife, the Bootstrap, and Other Resampling Plans*, (Philadelphia: Society for Industrial and Applied Mathematics)
- Foltz, C. B., Weymann, R. J., Peterson, B. M., Sun, L., Malkan, M. A., & Chaffee, F. H. Jr. 1986, *ApJ*, 307, 504
- Foltz, C. B., Chaffee, F. H. Jr., Hewett, P. C., MacAlpine, G. M., Turnshek, D. A., Weymann, R. J., & Anderson, S. F. 1987, *AJ*, 94, 1423
- Foltz, C. B., Chaffee, F. H. Jr., Hewett, P. C., Weymann, R. J., Anderson, S. F., & MacAlpine, G. M. 1989, *AJ*, 98, 1959
- Giallongo, E., Cristiani, S., D'Odorico, S., Fontana, A., & Savaglio, S. 1996, *ApJ*, 466, 46
- Hernquist, L., Katz, N., Weinberg, D., & Miralda-Escudé, J. 1996, *ApJ*, 457, L51
- Hewitt, A. & Burbidge, G. 1993, *ApJS*, 87, 451
- Hu, E. M., Kim, T. -S., Cowie, L. L., Songaila, A., & Rauch, M. 1995, *AJ*, 110, 1526
- Jannuzi, B. T., Bahcall, J. N., Bergeron, J., Boksenberg, A., Hartig, G., Kirhakos, S., Sargent, W. L. W., Savage, B. D., Schneider, D. P., Turnshek, D. A., Weymann, R. J., & Wolfe, A. M. 1998, *ApJS*, 118, 1
- Junkkarinen, V., Hewitt, A., & Burbidge, G. 1991, *ApJS*, 77, 203
- Kim, T.- S., Hu, E. M., Cowie, L. L., & Songaila, A. 1997, *AJ*, 114, 1
- Koratkar, A. P., Kinney, A. L., & Bohlin, R. C. 1992, *ApJ*, 400, 435
- Kunth, D., Sargent, W. L. W., & Kowal, C. 1981, *ã*, 44, 229
- Lanzetta, K. M., Turnshek, D. A., & Wolfe, A. M. 1987, *ApJ*, 322, 739 (LTW87)
- Lanzetta, K. M. 1991, *ApJ*, 375, 1
- Lanzetta, K. M., Turnshek, D. A., & Sandoval J. 1993, *ApJS*, 84, 109
- Lanzetta, K. M., Bowen, D. V., Tytler, D., Webb, J. K. 1995, *ApJ*, 442, 538
- Lanzetta, K. M., Wolfe, A. M., & Turnshek, D. A. 1995, *ApJ*, 440, 435
- Lanzetta, K. M., Webb, J. K., & Barcons, X. 1996, *ApJ*, 456, L17
- Lesser, M. 1994, *Proc. SPIE*, 2198, 782
- Lu, L., Wolfe, A. M., & Turnshek, D. A. 1991, *ApJ*, 367, 19 (LWT)
- Lynds, C. R. 1971, *ApJ*, 164, L73
- Miralda-Escudé, J., Cen, R., Ostriker, J. P., Rauch, M., 1996, *ApJ*, 471, 582
- Morton, D. C., York, D. G., & Jenkins, E. B. 1988, *ApJS*, 68, 449
- Murdoch, H. S., Hunstead, R. W., Pettini, M., & Blades, J. C. 1986, *ApJ*, 309, 19 (MHPB)
- Nelson, B. O. & Malkan, M. A. 1992, *ApJS*, 82, 447
- Oemler, A., Jr. & Lynds, C. R. 1975, *ApJ*, 199, 558
- Reisenegger, A. & Miralda-Escudé, J. 1995, *ApJ*, 449, 476
- Sargent, W. L. S., Young, P. J., Boksenberg, A., Carswell, R. F., & Whelan, J. A. J. 1979, *ApJ*, 230, 49
- Sargent, W. L. S., Young, P. J., Boksenberg, A., & Tytler, D. 1980, *ApJS*, 42, 41
- Sargent, W. L. S., Young, P. J., & Boksenberg, A. 1982, *ApJ*, 252, 54
- Sargent, W. L. S., Boksenberg, A. & Steidel, C. C. 1988, *ApJS*, 68, 539 (SBS88)
- Sargent, W. L. S., Steidel, C. C., & Boksenberg, A. 1989, *ApJS*, 69, 703
- Schmidt, M. & Olsen, E. T. 1968, *AJ*, 73, S117
- Scott, J., Bechtold, J., Dobrzycki, A., & Kulkarni, V. 2000, *ApJS*, in press (Paper II)
- Songaila, A. & Cowie, L. L. 1996, *AJ*, 112, 335
- Steidel, C. 1990, *ApJS*, 74, 37
- Steidel, C. & Sargent, W. L. S. 1991, *ApJ*, 382, 433
- Steidel, C. & Sargent, W. L. S. 1992, *ApJS*, 80, 1 (SS92)
- Stengler-Larrea, E. A., Boksenberg, A., Steidel, C. C., Sargent, W. L. W., Bahcall, J. N., Bergeron, J., Hartig, G., Jannuzi, B. T., Kirhakos, S., Savage, B. D., Schneider, D. P., Turnshek, D. A., & Weymann, R. J. 1995, *ApJ*, 444, 64
- Stickel, M. & Kühr, H. 1993, *A&AS*, 100, 395
- Storrie-Lombardi, L. J., M^cMahon, R. G., Irwin, M. J., & Hazard, C. 1994, *ApJ*, 427, L13
- Storrie-Lombardi, L. J. 1995, in *Proc. of the ESO Workshop on QSO Absorption Lines*, ed. G. Meylan (Berlin: Springer), 47
- Thompson, D. J., Djorgovski, S., & Weir, W. N. 1989 *PASP*, 101, 1065
- Tytler, D., Fan, X. -M., Junkkarinen, V. T., & Cohen, R. D. 1993, *AJ*, 106, 426 (T93)
- Uomoto, A. 1984, *ApJ*, 284, 497
- Weinberg, D. H., Croft, R. A. C., Hernquist, L., Katz, N., & Pettini, M. 1999, *ApJ*, 522, 563
- Weymann, R. J., Williams, R. E., Peterson, B. M., & Turnshek, D. A. 1979, *ApJ*, 234, 33
- Weymann, R. J., Carswell, R. F., & Smith, M. G. 1981, *ARA&A*, 19, 41
- Weymann, R. J., Jannuzi, B. T., Lu, L., Bahcall, J. N., Bergeron, J., Boksenberg, A., Hartig, G., Kirhakos, S., Sargent, W. L. W., Savage, B. D., Schneider, D. P., Turnshek, D. A., & Wolfe, A. M. 1998, *ApJ*, 506, 1
- Williger, G. M., Baldwin, J. A., Carswell, R. F., Cooke, A. J., Hazard, C., Irwin, M. J., M^cMahon, R. G., & Storrie-Lombardi, L. J. 1994, *ApJ*, 428, 574
- Wolfe, A. M., Turnshek, D. A., Smith, H. E., Cohen, R. D. 1986, *ApJS*, 61, 249 (W86)
- Wolfe, A. M., Lanzetta, K. M., Foltz, C. B., & Chaffee, F. H. 1995, *ApJ*, 454, 698
- York, D. G., Yanny, B., Crotts, A., Carilli, C., Garrison, E., & Matheson, L. 1991, *MNRAS*, 250, 24
- Young, P., Sargent, W. L. S., Boksenberg, A., Carswell, R. F., & Whelan, J. A. J. 1979, *ApJ*, 228, 891
- Young, P., Sargent, W. L. S., & Boksenberg, A. 1982a, *ApJ*, 252, 10
- Young, P., Sargent, W. L. S., & Boksenberg, A. 1982b, *ApJS*, 48, 455 (YSB82)

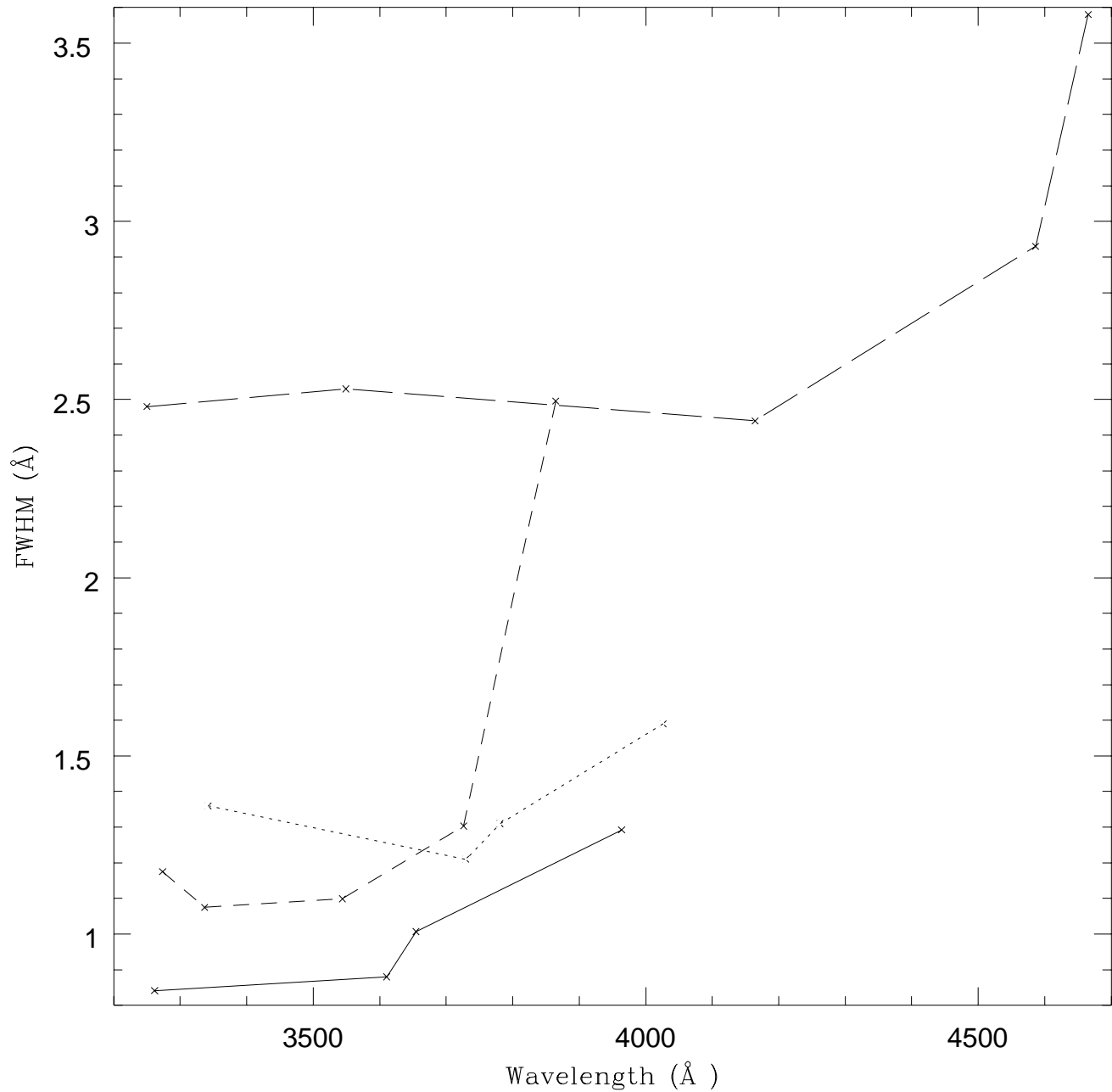


FIG. 1.— FWHM of comparison lines versus wavelength for four separate instrumental setups listed in Table 1: solid line- (1) Big Blue Reticon, 832 l mm^{-1} 2^{nd} order, $1'' \times 3''$ slit; short dashed line- (2) 3Kx1K CCD, 832 l mm^{-1} 2^{nd} order, $1'' \times 180''$ slit; dotted line- Same as previous setup but with improved field flattener (see text); long dashed line- (3) 3Kx1K CCD, 800 lmm^{-1} 1^{st} order, $1'' \times 180''$ slit

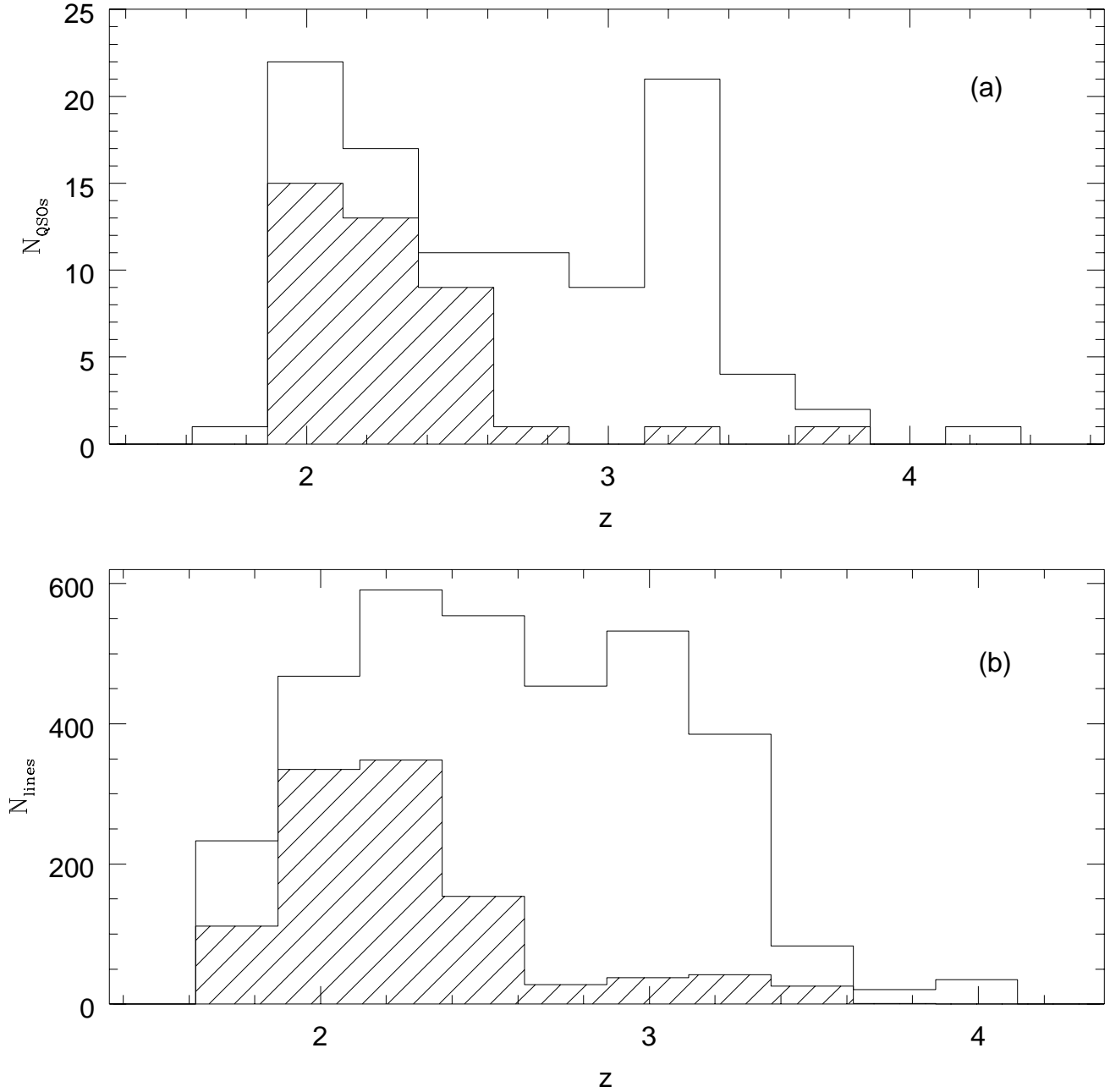


FIG. 2.— (a) Histogram of 99 QSO redshifts, includes QSOs presented in this paper (shaded region) and objects from the literature; (b) Histogram of 3356 absorption line redshifts from QSOs presented in this paper (shaded region) and objects from the literature, using a variable equivalent width threshold, includes all lines between each QSO's $\text{Ly}\beta$ and $\text{Ly}\alpha$ emission lines

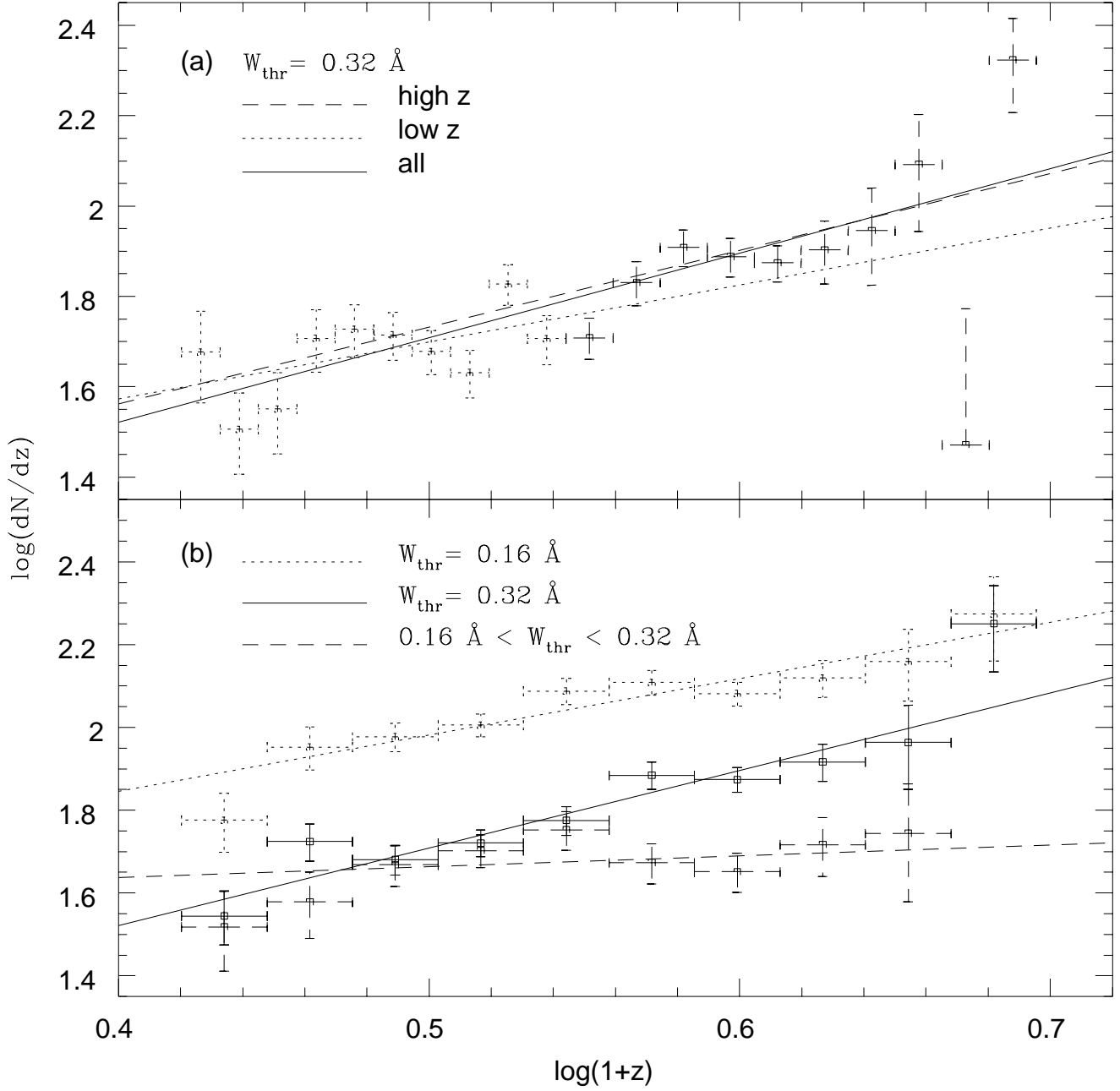


FIG. 3.— (a) $\log(dN/dz)$ vs. $\log(1+z)$ for $z < 2.5$ (dotted line), $z > 2.5$ (dashed line), and all lines (solid line) each using a fixed threshold of 0.32 \AA ; (b) $\log(dN/dz)$ vs. $\log(1+z)$ for different equivalent width thresholds: $W > 0.16 \text{ \AA}$ (dotted line); $W > 0.32 \text{ \AA}$ (solid line); $0.16 \text{ \AA} < W < 0.32 \text{ \AA}$ (dashed line)

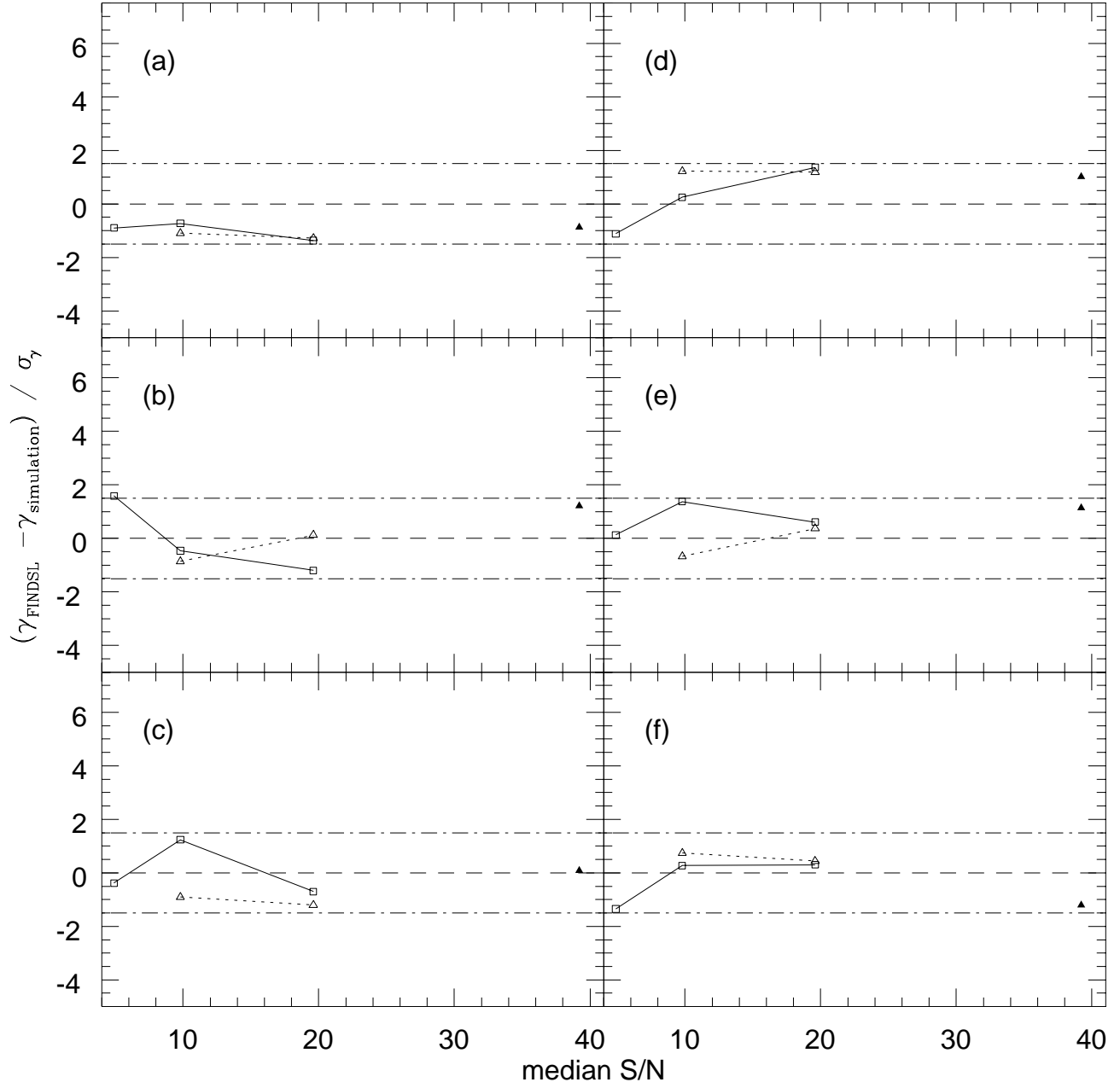


FIG. 4.— $(\gamma_{\text{FINDSL}} - \gamma_{\text{simulation}}) / \sigma_{\gamma}$ vs. median signal-to-noise, open squares and solid line- data resolution, $\sim 1 \text{ \AA}$; open triangles and dotted line- $\Delta\lambda \sim 0.7 \text{ \AA}$; filled triangles- $\Delta\lambda \sim 0.2 \text{ \AA}$: (a) variable threshold; (b) variable threshold, $z < 2.5$; (c) variable threshold, $z > 2.5$; (d) $W > 0.32 \text{ \AA}$; (e) $W > 0.32 \text{ \AA}$, $z < 2.5$; (f) $W > 0.32 \text{ \AA}$, $z > 2.5$

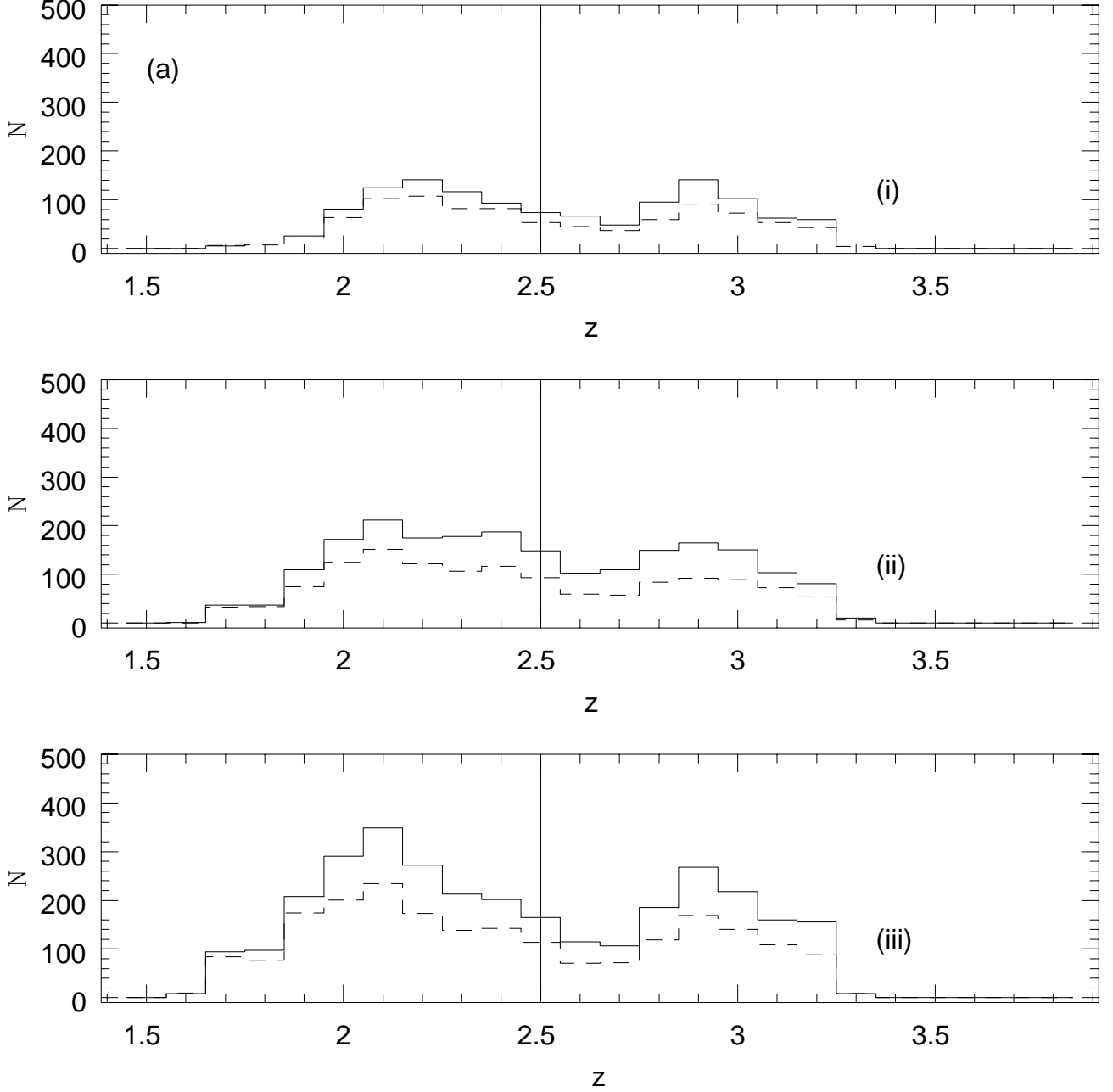
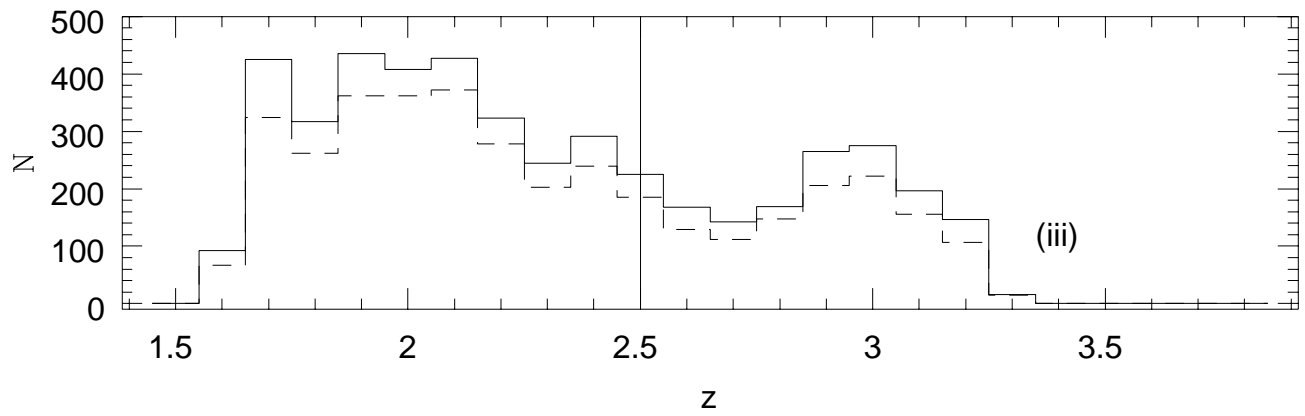
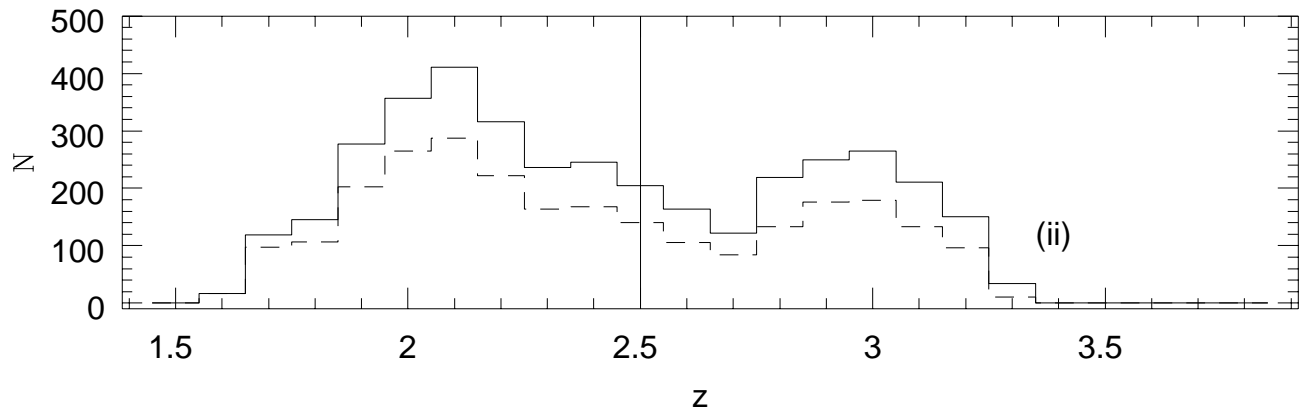
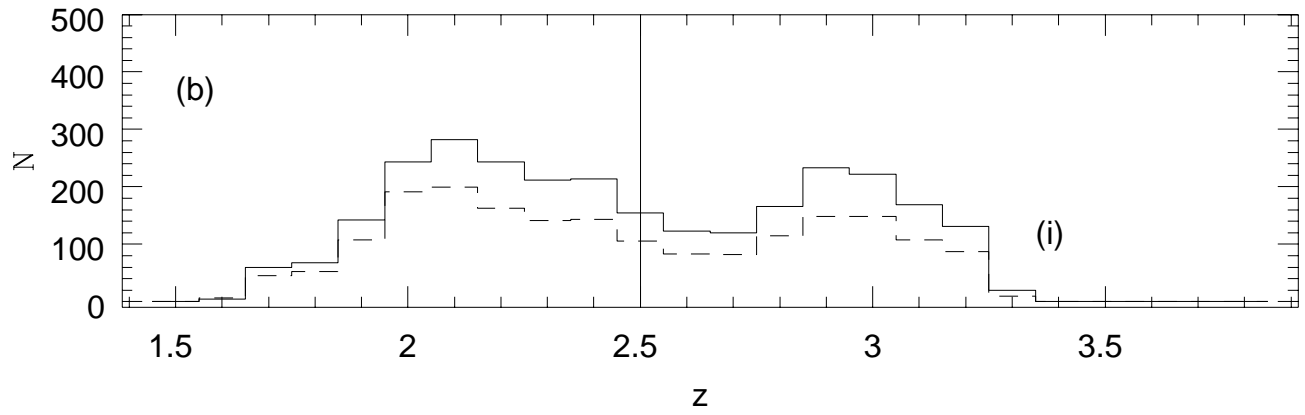
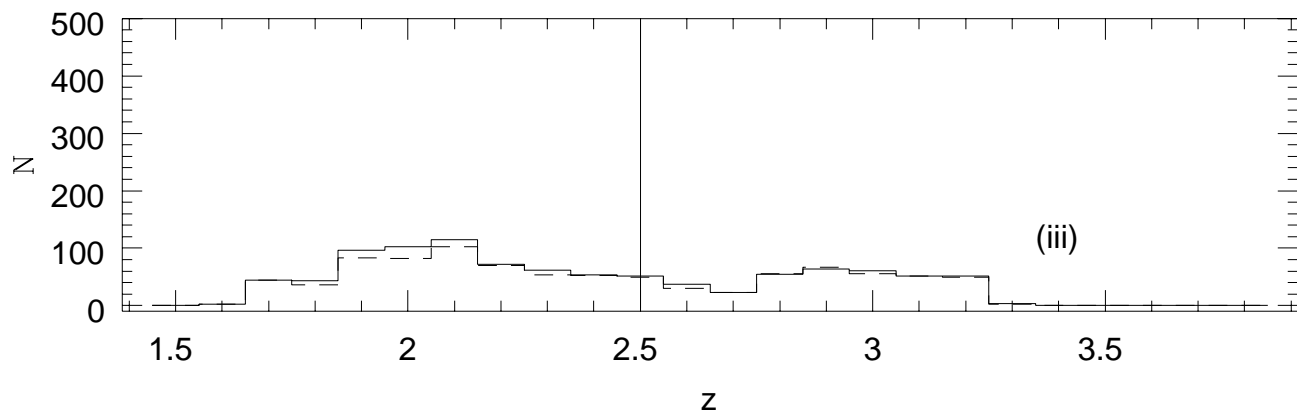
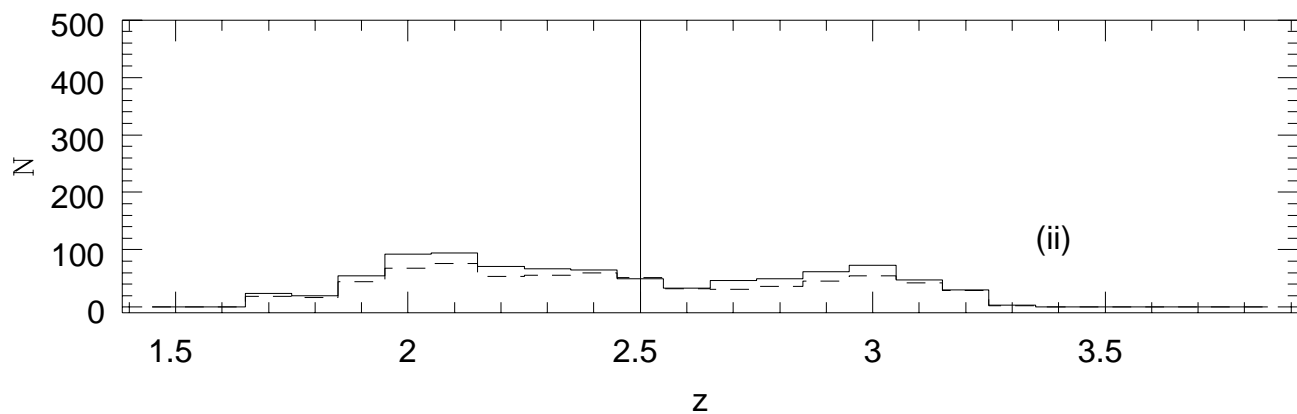
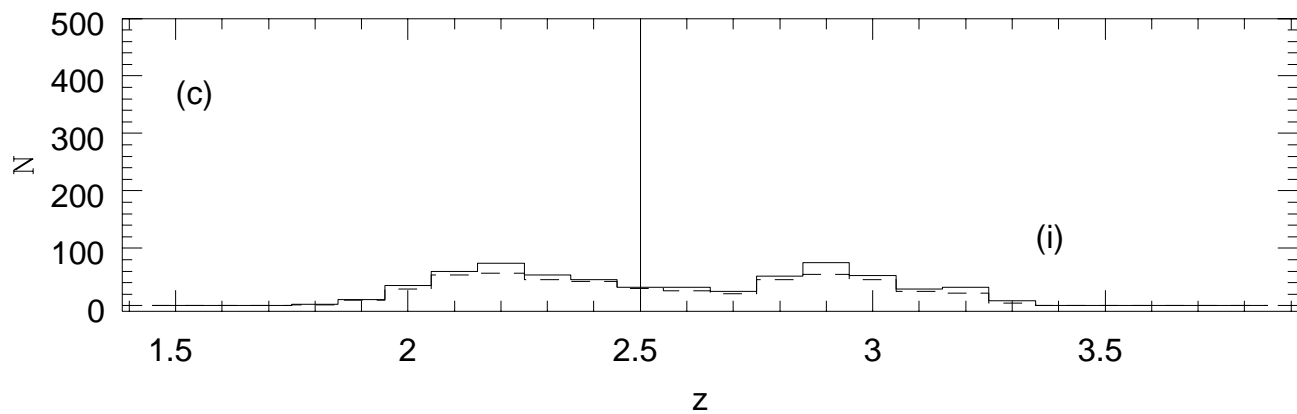
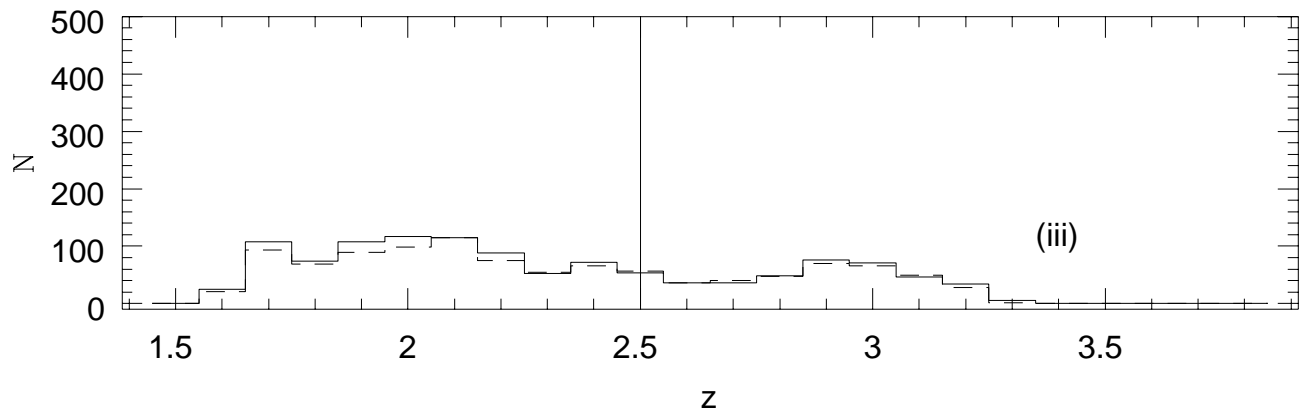
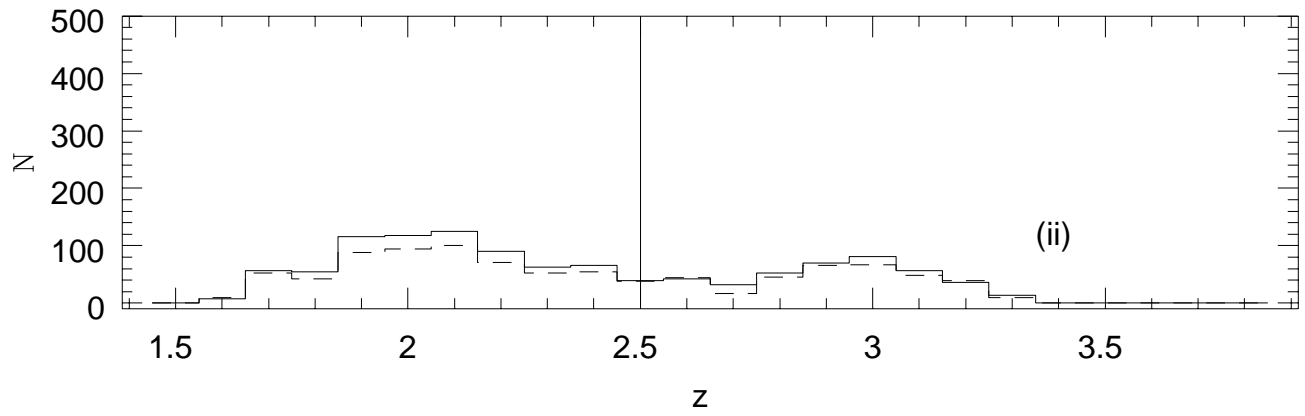
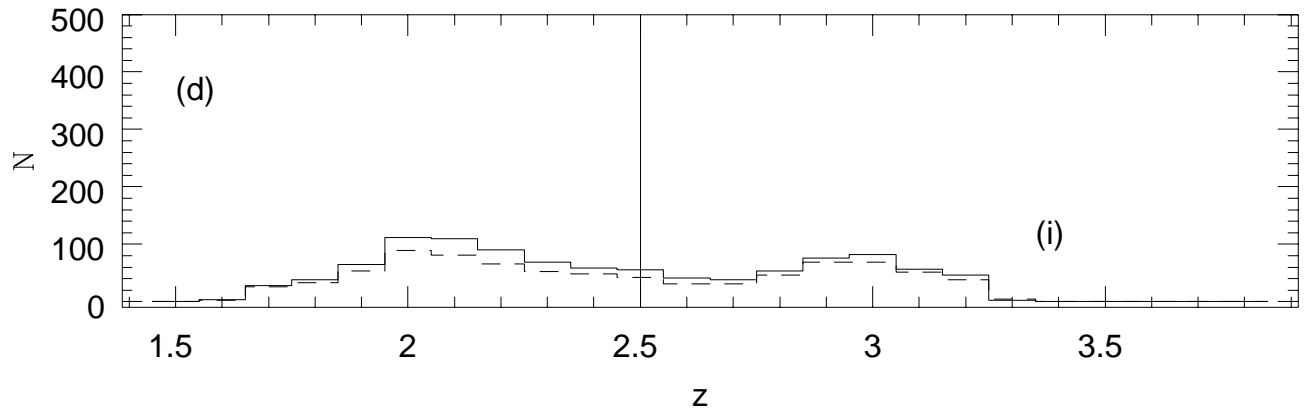


FIG. 5.— Histograms of the line distribution used to solve for the simulation input γ (solid line) and FINDSL output γ (dashed line); vertical line at $z=2.5$ marks the division between low z and high z solutions for γ in Fig. 4: (a) variable threshold, $\Delta\lambda \sim 1 \text{ \AA}$ - (i) median S/N ~ 5 , (ii) median S/N ~ 10 , (iii) median S/N ~ 20 ; (b) variable threshold, $\Delta\lambda \sim 0.7 \text{ \AA}$ - (i) median S/N ~ 10 , (ii) median S/N ~ 20 , (iii) $\Delta\lambda \sim 0.2 \text{ \AA}$, median S/N ~ 40 ; (c) constant threshold, $\Delta\lambda \sim 1 \text{ \AA}$ - (i) median S/N ~ 5 , (ii) median S/N ~ 10 , (iii) median S/N ~ 20 ; (d) constant threshold, $\Delta\lambda \sim 0.7 \text{ \AA}$ - (i) median S/N ~ 10 , (ii) median S/N ~ 20 , (iii) $\Delta\lambda \sim 0.2 \text{ \AA}$, median S/N ~ 40







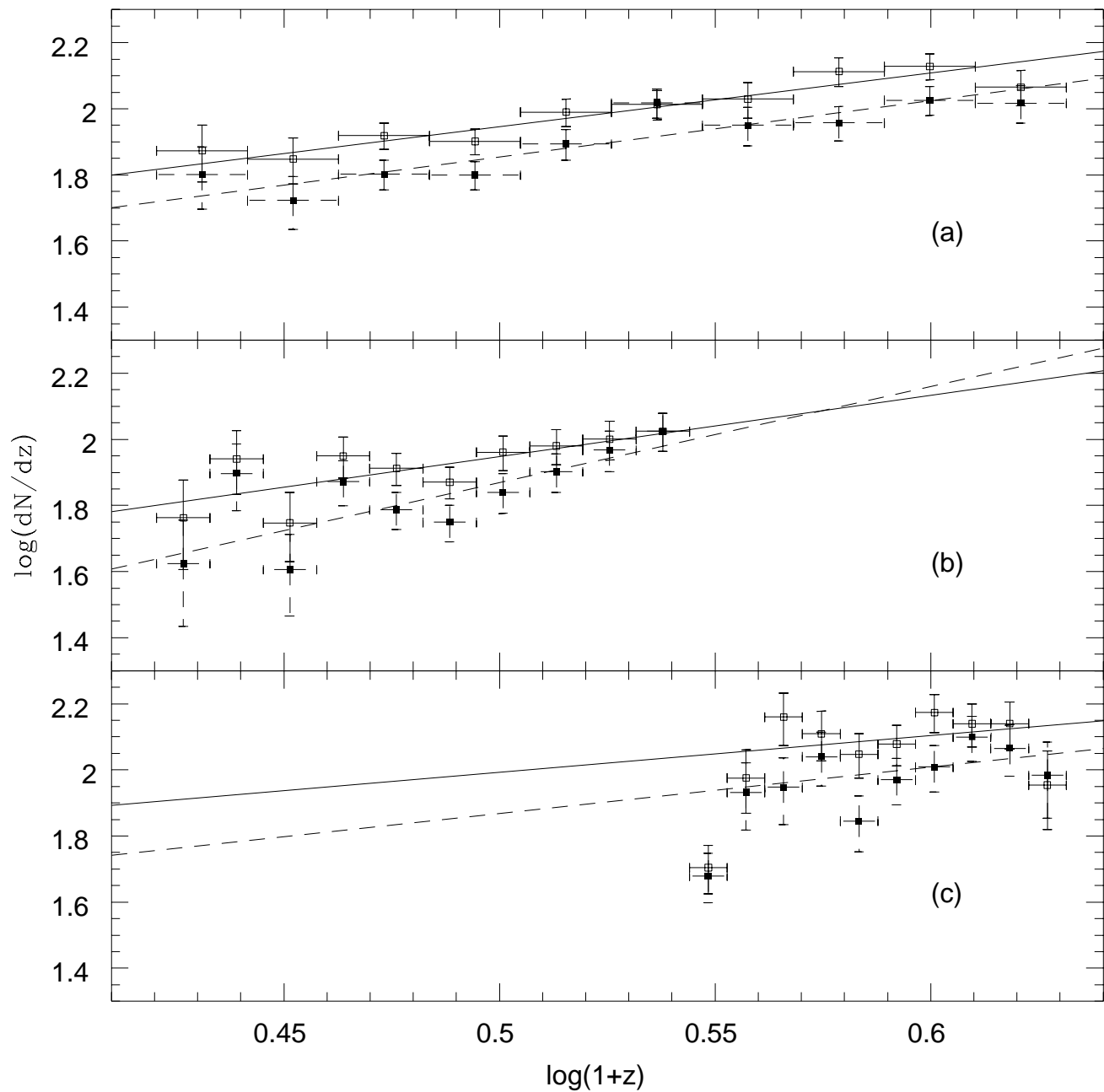


FIG. 6.— $\log(dN/dz)$ vs. $\log(1+z)$ for the data resolution, data S/N simulation line lists (solid line) and FINDSL line lists (dashed line), for lines with $W > 0.32 \text{ \AA}$; (a) all z ; (b) $z < 2.5$; (c) $z > 2.5$

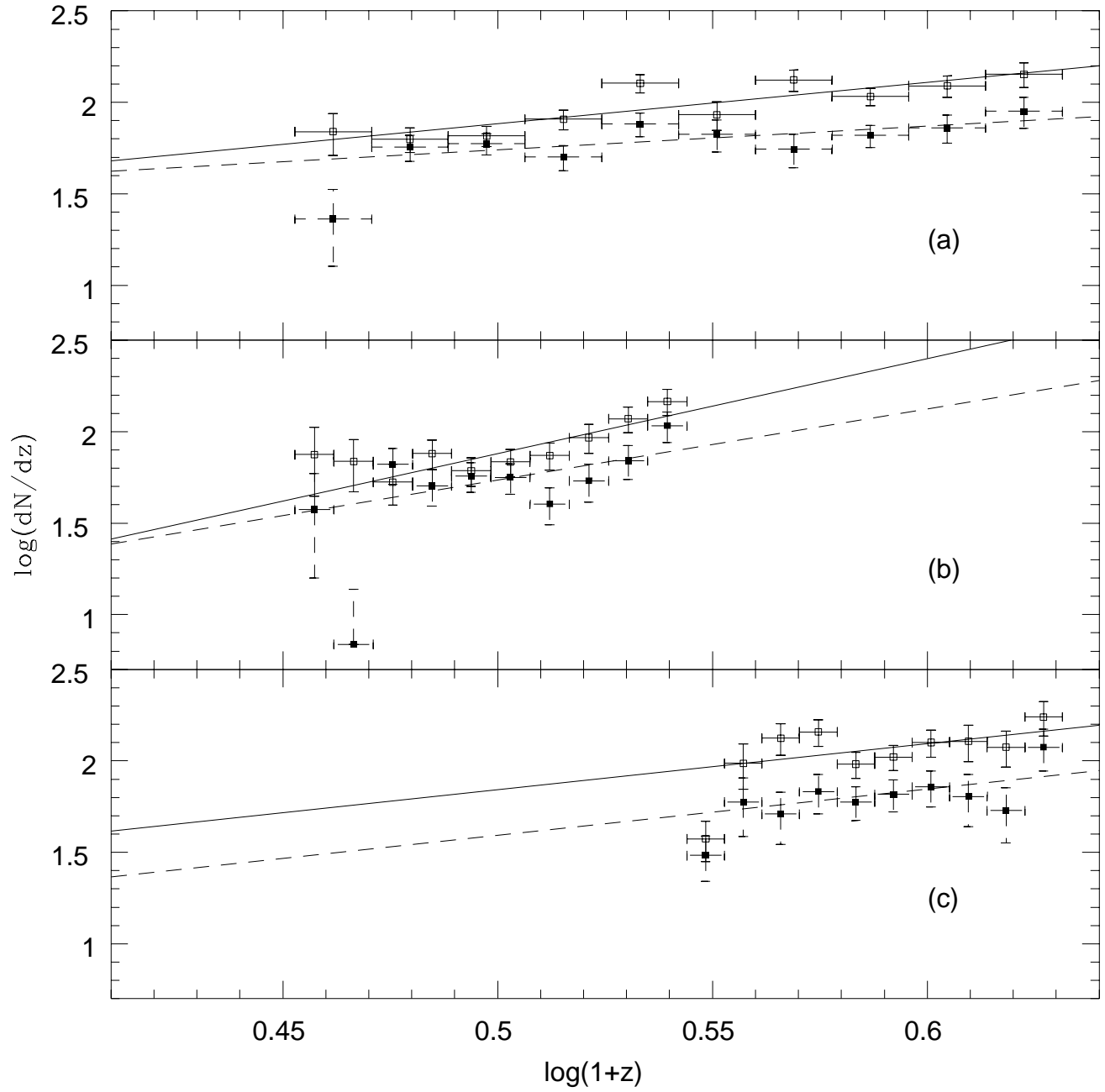


FIG. 7.— Same as Figure 6, but for lines with $0.16 \text{ \AA} < W < 0.32 \text{ \AA}$.

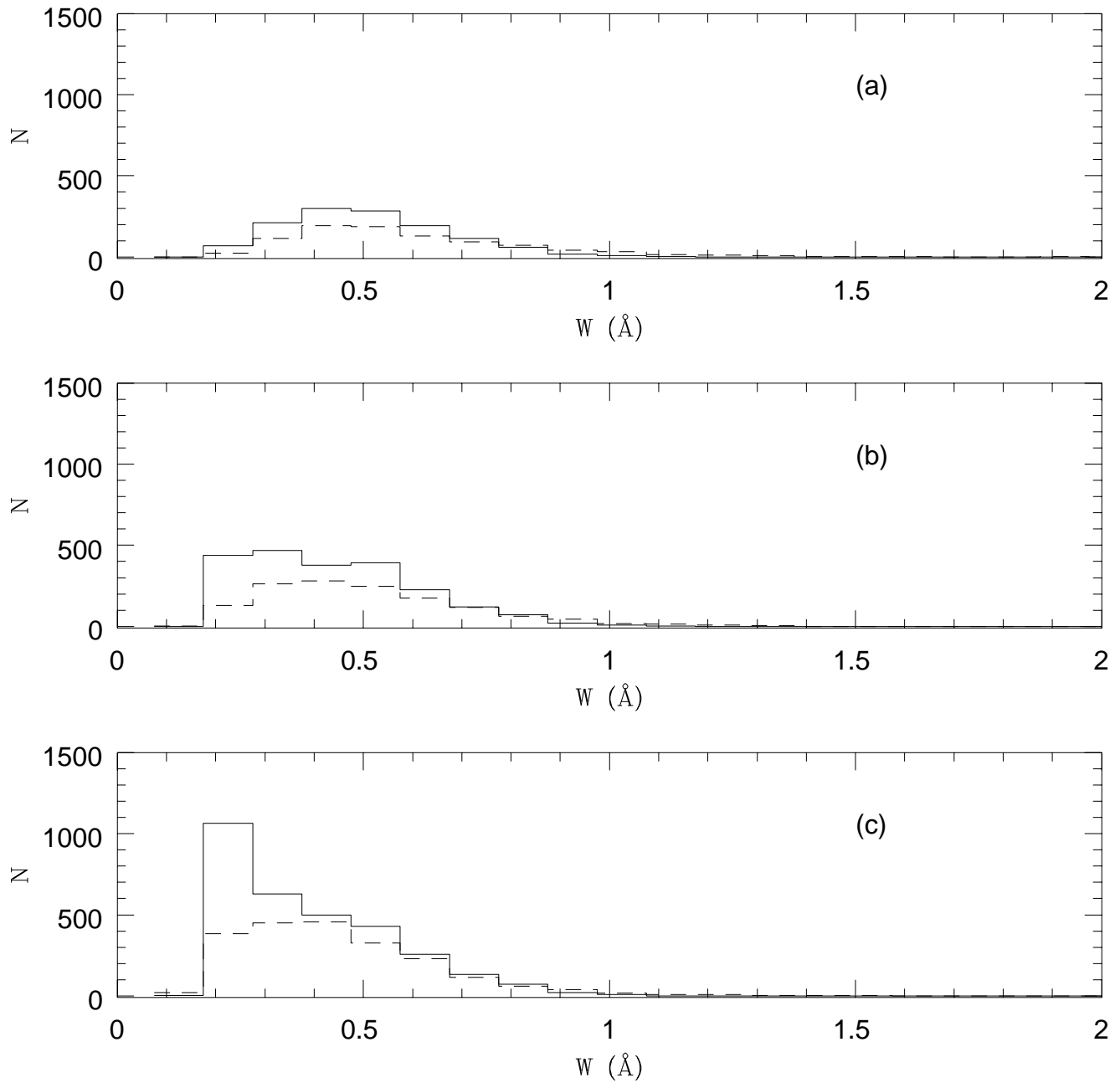


FIG. 8.— Rest equivalent width distribution of lines in the data resolution, data S/N simulation line lists (solid line) and in the FINDSL line lists (dashed line), variable threshold case: (a) median S/N ~ 5 ; (b) median S/N ~ 10 ; (c) median S/N ~ 20

TABLE 1
SUMMARY OF QSO ABSORPTION LINE SPECTRA OBSERVATIONS

QSO	Alternate Name	z_{em}	Ref. (a)	m_V (b)	Instr. (c)	Date	Total Exposure (seconds)	Wavelength (\AA)
0006+020		2.34	1	17.5	2	15Nov93	7200	3200-4088
0027+018	UM 247	2.31	2	18.9	1	25Oct92	3600	3136-4118
0037-018	UM 264	2.34	1	18.0	2	7Jan94	7200	3205-4109
0049+007	UM 287	2.27	3	17.8	1	23-25Oct92	9600	3150-4111
0123+257	PKS	2.37	3	17.5	2	16Nov93	9000	3198-4094
0150-202	UM 675	2.14	4	17.1	1	24-25Oct92	6000	3173-4126
0153+744	S5	2.34	3	16.0	2	15Nov93	3600	3192-4088
0226-038	PKS	2.07	3	16.9	2	16Nov93	3000	3198-4095
0348+061		2.05	4	17.6	1	25Oct92	2400	3130-4112
0400+258	B2	2.10	1	18.0	2	7Jan94	3000	3209- 4121
0747+613		2.49	1	17.5	1	25Oct92	3600	3323-4269
0836+710	S5	2.21	3	16.5	2	15Nov93	3600	3192-4088
0848+155		2.01	4	17.7	2	15Nov93	3600	3192-4088
0936+368	CSO 233	2.02	1	17.0	2	4Apr94	3600	3176-4058
0952+338	CSO 239	2.50	1	17.0	2	7Jan94	5400	3486-4389
0955+472	PC	2.48	1	17.7	2	7Jan94	3600	3486-4389
0956+122		3.30	1	17.5	2	7Jan94	3600	4394-5293
1009+299	CSO 38	2.63	1	16.0	2	7Jan94	3600	3622-4525
1207+399		2.45	3	17.5	3	5Apr94	900	3201-4824

TABLE 1—*Continued*

QSO	Alternate Name	z_{em}	Ref. (a)	m_V (b)	Instr. (c)	Date	Total Exposure (seconds)	Wavelength (\AA)
1210+175		2.56	1	17.4	2	4June94	3600	3572-4453
1231+294	CSO 151	2.01	1	16.0	2	12Mar94	1800	3172-4053
1323-107	POX188	2.36	5	17.0	2	4June94	5400	3200-4087
1329+412	PG	1.93	1	16.3	2	3June94	1800	3202-4087
1337+285		2.54	1	17.1	2	3June94	3600	3574-4455
1346-036		2.36	3	17.2	2	18Jul93	3600	3275-4155
1358+115		2.58	1	16.5	2	18Jul93	3600	3547-4424
1406+492	CSO 609	2.16	1	17.0	2	3-4June94	3400	3201-4085
1408+009	UM 645	2.26	3	18.0	3	5Apr94	900	3200-4807
1421+330	MKN 679	1.90	4	16.7	2	4June94	1800	3200-4084
1422+231		3.62	3	16.5	2	16-17Jul93	1800	4853-5716
1435+638		2.06	3	15.0	2	16-17Jul93	7200	3100-3942
1603+383	HS	2.51	6	16.9	4	12-13Apr97	3300	3532-5045
1604+290	KP 63	1.96	1	17.0	2	18Jul93	3600	3100-3943
1715+535	PG	1.93	4	16.3	2	16-17Jul93	9000	3100-3938
2134+004	PKS	1.94	1	17.5	1	24-25Oct92	7200	3173-4125
2251+244	PKS	2.35	3	17.8	2	16Nov93	12000	3200-4093
2254+022	PKS	2.09	4	17.0	2	16-17Jul93	7200	3100-3936
2310+385	UT	2.18	3	17.5	1	25Oct92	1200	3200-4118

TABLE 1—*Continued*

QSO	Alternate Name	z_{em}	Ref. (a)	m_V (b)	Instr. (c)	Date	Total Exposure (seconds)	Wavelength (\AA)
2320+079	PKS	2.08	1	17.5	2	17Jul93	5400	3160-3940
2329-020	UM 164	1.89	1	17.0	2	18Jul93	3600	3060-3943

^a(1) this paper, from Ly α emission; (2) Baker et al. 1994; (3) Scott et al. (2000) and references therein; (4) Steidel & Sargent 1991; (5) Hewitt & Burbidge 1993; (6) Dobrzycki, Engels, & Hagen (1999)

^bas listed in Hewitt & Burbidge 1993, with the exception of 1603+383 for which V was calculated from the flux- calibrated spectrum (unpublished)

^cInstrument Set-up: (1) Big Blue Reticon, 832 l mm^{-1} 2^{nd} order, $1'' \times 3''$ slit; (2) 3Kx1K CCD, 832 l mm^{-1} 2^{nd} order, $1'' \times 180''$ slit; (3) 3Kx1K CCD, 800 lmm^{-1} 1^{st} order, $1'' \times 180''$ slit; (4) 3Kx1K CCD, 1200 lmm^{-1} 1^{st} order, $1'' \times 3''$ slit

TABLE 2
QSO SPECTRA FROM THE LITERATURE

QSO	z_{em}	Reference
0000-263	4.111	1
0001+087	3.243	1
0002+051	1.899	2
0002-422	2.763	3,4
0014+813	3.384	1,5
0029+073	3.294	1
0058+019	1.959	6
0100+130	2.690	4
0114-089	3.205	1,5
0119-046	1.937	7
0142-100	2.727	6
0237-233	2.222	6
0256-000	3.374	1,5
0301-005	3.223	1
0302-003	3.286	1,5
0334-204	3.126	1
0421+019	2.051	2
0424-131	2.166	6
0453-423	2.656	3,4
0636+680	3.174	1,5
0731+653	3.033	1
0831+128	2.739	1,5
0837+109	3.326	6
0848+163	1.925	6
0905+151	3.173	1
0913+072	2.784	1,5
0938+119	3.192	1
1017+280	1.928	6
1033+137	3.092	1
1115+080	1.725	2
1159+124	3.502	6
1206+119	3.108	1,5
1208+101	3.822	1
1215+333	2.606	1,5
1225-017	2.831	1,5
1225+317	2.200	4
1247+267	2.039	6
1315+472	2.590	1,5
1334-005	2.842	1,5
1400+114	3.177	1
1402+044	3.206	1
1410+096	3.313	1
1442+101	3.554	1
1451+123	3.251	1
1511+091	2.878	6
1512+132	3.120	1
1548+092	2.748	1,5
1601+182	3.227	1
1602+178	2.989	1
1607+183	3.134	1,5
1614+051	3.216	1
1623+269	2.526	1,5
1700+642	2.744	1,5
1738+350	3.239	1
1946+770	3.020	5
2126-158	3.280	4

TABLE 2—*Continued*

QSO	z_{em}	Reference
2233+131	3.295	1
2233+136	3.209	1
2311-036	3.041	1

^aReferences: (1)Bechtold 1994; (2) Young, Sargent, & Boksenberg 1982a; (3)Sargent et al. 1979; (4) Sargent et al. 1980; (5) Dobrzycki & Bechtold 1996; (6) Sargent, Boksenberg, & Steidel 1988; (7) Sargent, Young, & Boksenberg 1982

TABLE 3
MAXIMUM LIKELIHOOD ESTIMATIONS OF γ, W^* , AND \mathcal{A}_0

Sample (a)	No. lines	W limit	γ (b)	W^* (\AA) (b)	\mathcal{A}_0 (b)	P_{KS}
1.....	1	2079	variable	1.23 ± 0.16	0.313 ± 0.006	-
2.....	1	1295	$W > 0.16\text{\AA}$	1.35 ± 0.21	0.300 ± 0.008	20.1
3.....	1	1131	$W > 0.32\text{\AA}$	1.88 ± 0.22	0.307 ± 0.009	5.78
4.....	1	1208	$0.16 < W < 1.00\text{\AA}$	1.11 ± 0.22	0.238 ± 0.006	25.4
5.....	1	1007	$0.32 < W < 1.00\text{\AA}$	1.59 ± 0.24	0.226 ± 0.007	7.47
6.....	1	555	$0.16 < W < 0.32\text{\AA}$	0.26 ± 0.33	0.075 ± 0.003	34.1
7.....	2	1084	variable	1.57 ± 0.42	0.284 ± 0.008	-
8.....	2	605	$W > 0.16\text{\AA}$	2.42 ± 0.62	0.257 ± 0.010	5.86
9.....	2	534	$W > 0.32\text{\AA}$	1.30 ± 0.60	0.282 ± 0.012	11.1
10.....	2	578	$0.16 < W < 1.00\text{\AA}$	2.26 ± 0.63	0.218 ± 0.009	6.77
11.....	2	491	$0.32 < W < 1.00\text{\AA}$	1.07 ± 0.63	0.229 ± 0.010	13.2
12.....	2	298	$0.16 < W < 0.32\text{\AA}$	2.47 ± 0.88	0.073 ± 0.004	2.72
13.....	3	995	variable	0.64 ± 0.47	0.348 ± 0.010	-
14.....	3	690	$W > 0.16\text{\AA}$	0.46 ± 0.55	0.338 ± 0.012	67.9
15.....	3	597	$W > 0.32\text{\AA}$	1.69 ± 0.60	0.330 ± 0.013	7.62
16.....	3	630	$0.16 < W < 1.00\text{\AA}$	-0.05 ± 0.58	0.256 ± 0.010	125.
17.....	3	516	$0.32 < W < 1.00\text{\AA}$	1.26 ± 0.65	0.223 ± 0.009	11.8
18.....	3	257	$0.16 < W < 0.32\text{\AA}$	-1.22 ± 0.94	0.077 ± 0.004	251.

^a(1)entire sample; (2) low redshift subsample; (3) high redshift subsample

^bsee Equ. 2

TABLE 4
SIMULATION RESULTS FOR γ

$\Delta\lambda$ (\AA) (1)	median S/N (2)	z range (3)	W limit (4)	$\gamma_{\text{simulation}}$ (5)	γ_{FINDSL} (6)
1.0	4.9	all z	variable	1.99±0.25	1.71±0.30
1.0	4.9	z < 2.5	variable	1.47±0.74	2.82±0.84
1.0	4.9	z > 2.5	variable	2.25±0.76	1.88±0.98
1.0	4.9	all z	0.32 \AA	2.33±0.37	1.86±0.42
1.0	4.9	z < 2.5	0.32 \AA	2.24±1.19	2.42±1.32
1.0	4.9	z > 2.5	0.32 \AA	3.12±1.12	1.38±1.28
1.0	9.8	all z	variable	1.63±0.18	1.47±0.22
1.0	9.8	z < 2.5	variable	2.61±0.47	2.36±0.54
1.0	9.8	z > 2.5	variable	0.36±0.61	1.35±0.79
1.0	9.8	all z	0.32 \AA	1.62±0.27	1.70±0.30
1.0	9.8	z < 2.5	0.32 \AA	1.85±0.68	2.90±0.76
1.0	9.8	z > 2.5	0.32 \AA	1.10±0.97	1.40±1.08
1.0	9.8	all z	0.16 < W < 0.32 \AA	2.25±0.40	1.30±0.49
1.0	9.8	z < 2.5	0.16 < W < 0.32 \AA	5.18±1.26	3.88±1.50
1.0	9.8	z > 2.5	0.16 < W < 0.32 \AA	2.51±1.23	2.52±1.68
1.0	19.6	all z	variable	1.91±0.14	1.67±0.17
1.0	19.6	z < 2.5	variable	1.82±0.34	1.33±0.40
1.0	19.6	z > 2.5	variable	3.34±0.53	2.87±0.66
1.0	19.6	all z	0.32 \AA	1.79±0.24	2.14±0.25
1.0	19.6	z < 2.5	0.32 \AA	1.48±0.57	1.86±0.61
1.0	19.6	z > 2.5	0.32 \AA	3.61±1.00	3.92±1.02
0.7	9.8	all z	variable	1.77±0.15	1.56±0.18
0.7	9.8	z < 2.5	variable	1.86±0.39	1.46±0.46
0.7	9.8	z > 2.5	variable	2.34±0.54	1.73±0.67
0.7	9.8	all z	0.32 \AA	2.11±0.24	2.44±0.27
0.7	9.8	z < 2.5	0.32 \AA	2.04±0.61	1.58±0.69
0.7	9.8	z > 2.5	0.32 \AA	2.38±0.92	3.12±1.01
0.7	19.6	all z	variable	1.76±0.12	1.56±0.15
0.7	19.6	z < 2.5	variable	1.98±0.30	2.02±0.35
0.7	19.6	z > 2.5	variable	2.42±0.49	1.68±0.61
0.7	19.6	all z	0.32 \AA	1.90±0.22	2.19±0.24
0.7	19.6	z < 2.5	0.32 \AA	1.69±0.52	1.90±0.57
0.7	19.6	z > 2.5	0.32 \AA	3.56±0.96	4.01±1.03
0.2	39.2	all z	variable	1.41±0.10	1.31±0.12
0.2	39.2	z < 2.5	variable	1.22±0.23	1.54±0.25
0.2	39.2	z > 2.5	variable	0.72±0.48	0.77±0.55
0.2	39.2	all z	0.32 \AA	1.68±0.21	1.91±0.21
0.2	39.2	z < 2.5	0.32 \AA	1.69±0.45	2.24±0.48
0.2	39.2	z > 2.5	0.32 \AA	0.86±0.96	-0.33±0.98